BRNO UNIVERSITY OF TECHNOLOGY

Faculty of Mechanical Engineering

MASTER'S THESIS

Brno, 2024 Bc. Giorgi Bliadze

BRNO UNIVERSITY OF TECHNOLOGY

VYSOKÉ UČENÍ TECHNICKÉ V BRNĚ

FACULTY OF MECHANICAL ENGINEERING

FAKULTA STROJNÍHO INŽENÝRSTVÍ

INSTITUTE OF AUTOMOTIVE ENGINEERING

ÚSTAV AUTOMOBILNÍHO A DOPRAVNÍHO INŽENÝRSTVÍ

LUBRICATION GAP OPTIMISATION OF HYDRODYNAMIC OIL-FILM JOURNAL BEARING

OPTIMALIZACE TVARU MAZACÍ MEZERY HYDRODYNAMICKÉHO OLEJOVÉHO RADIÁLNÍHO LOŽISKA

MASTER'S THESIS

DIPLOMOVÁ PRÁCE

AUTHOR — Bc. Giorgi Bliadze

AUTOR PRÁCE

SUPERVISOR — prof. Ing. Pavel Novotný, Ph.D.

VEDOUCÍ PRÁCE

BRNO 2024

BRNO UNIVERSITY OF TECHNOLOGY
FACULTY OF MECHANICAL ENGINEERING

Assignment Master's Thesis

Institut:	Institute of Automotive Engineering
Student:	**Bc. Giorgi Bliadze**
Degree programm:	Mechanical Engineering
Branch:	no specialisation
Supervisor:	**prof. Ing. Pavel Novotný, Ph.D.**
Academic year:	2024/25

As provided for by the Act No. 111/98 Coll. on higher education institutions and the BUT Study and Examination Regulations, the director of the Institute hereby assigns the following topic of Master's Thesis:

Lubrication Gap Optimisation of Hydrodynamic Oil–film Journal Bearing

Brief Description:

Hydrodynamic oil–film bearings are usually designed with consideration of their bearing capacity, friction losses, oil flow rates and other integral quantities, and only in selected operating conditions. The geometric shape of the lubrication gap is described analytically using several parameters. The work assumes finding the optimal values of these parameters. It is assumed that the result of the optimization, i.e. the journal bearing concept, will show better integral parameters, compared to the existing serially used bearing design. The main requirements are lower frictional losses while maintaining the load carrying capacity and not exceeding the limit flow and warming.

Master's Thesis goals:

Analysis of existing optimization methods and approaches suitable for solving the given problem.Methodology for optimizing the integral parameters of a journal hydrodynamic oil–film bearing.

Application of the methodology for the design of the journal bearing of a turbocharger underseveral operating conditions.

Recommended bibliography:

NOVOTNÝ, Pavel, Martin JONÁK a Jiří VACULA. Evolutionary Optimisation of the Thrust Bearing Considering Multiple Operating Conditions in Turbomachinery. International Journal of Mechanical Sciences. 2021, 195. ISSN 00207403.

NOVOTNÝ, Pavel, Jiří VACULA a Jozef HRABOVSKÝ. Solution strategy for increasing the efficiency of turbochargers by reducing energy losses in the lubrication system. Energy. 2021,236. ISSN 03605442.

STACHOWIAK, G. W. a A. W. BATCHELOR. Engineering Tribology. 3. vyd. Boston: ElsevierButterworth-Heinemann, 2005. ISBN 0-7506-7836-4.

NGUYEN-SCHÄFER, H. Rotordynamics of Automotive Turbochargers. Second Edition.Ludwigsburg, Germany: Springer, 2015. ISBN 978-3-319-17643-7.

Deadline for submission Master's Thesis is given by the Schedule of the Academic year 2024/25

In Brno,

L. S.

prof. Ing. Josef Štětina, Ph.D. Director of the Institute	doc. Ing. Jiří Hlinka, Ph.D.FME dean

Abstract

Hydrodynamic oil–film bearings are usually designed with consideration of their bearing capacity, friction losses, oil flow rates and other integral quantities, and only in selected operating conditions. The geometric shape of the lubrication gap is described analytically using several parameters. The work assumes finding the optimal values of these parameters. It is assumed that the result of the optimization, i.e. the journal bearing concept, will show better integral parameters, compared to the existing serially used bearing design. The main requirements are lower frictional losses while maintaining the load carrying capacity and not exceeding the limit flow and warming.

Key words

Optimization, bearing, turbocharger, genetic algorithms, lubrication.

Bibliographic citation

Citation of the printed work:

BLIADZE, Giorgi. *Optimization of the lubrication gap shape of a hydrodynamic oil radial bearing*. Brno, 2025. Available also from: https://www.vut.cz/studenti/zav-prace/detail/162489. Thesis. Brno University of Technology, Faculty of Mechanical Engineering, Institute of Automotive and Transportation Engineering. Thesis supervisor Pavel Novotný.

Citation of the electronic source:

BLIADZE, Giorgi. *Optimization of the Lubrication Gap Shape of a Hydrodynamic Oil Radial Bearing* [online]. Brno, 2025 [cit. 2024-08-30]. Available from: https://www.vut.cz/studenti/zav-prace/detail/162489. Thesis. Brno University of Technology, Faculty of Mechanical Engineering, Institute of Automotive and Transportation Engineering. Thesis supervisor Pavel Novotný.

DECLARATION OF AUTHENTICITY

I thus certify that I worked freely and without outside help to write my master's thesis, "Lubrication Gap Optimisation of Hydrodynamic Oil–film Journal Bearing." I have properly cited every paragraph in the thesis that comes from outside sources, including any graphics, tables, and the like. I prepared this thesis independently under my supervision prof. Ing. Pavel Novotný, Ph.D. and I did not utilise any other sources but those included in the bibliography. No other degree program has ever received this thesis in its current or comparable form.

31. 08. 2024 .....

Date

Giorgi Bliadze

ACKNOWLEDGEMENT

I express my gratitude to my supervisor, professor Ing. Pavel Novotný, Ph.D., for his benevolent counsel, support, and direction throughout the entirety of my thesis preparation.

Table of Contents

1 Introduction

The combustion engines are widely used in various industries, such as power generation, construction, agriculture, transportation etc. This device was developed and improved over time. One of the determining factors of its efficiency is the turbocharger, which improved the quality of fuel combustion and gave us much greater power for the same fuel volume. This allowed us to reduce the size and therefore the mass of the engines. It is worth noting the fact that the operation of turbochargers depends on the exhaust gases, because it is at the expense of these gases that the turbine of the turbocharger rotates, which in turn sets the compressor in motion [4, 46]. The introduction of turbochargers in internal combustion engines not only resulted in an increase in the technical characteristics of the engine, such as rightsizing it with respect to the highest efficiency possible, but also significantly reduced the release of incomplete combustion products into the atmosphere [19]. This is directly because, thanks to the turbocharger, it was possible to supply high-pressure atmospheric air to the combustion chamber of the engine. This is ensured by the turbocharger compressor, since it can draw much more air under high pressure into the combustion chamber, which means that the air is compressed and has a greater density in the same volume than at atmospheric pressure, which in turn means more oxygen. More oxygen means a higher degree of complete combustion of the fuel and therefore more power [46]. So, considering all this, the turbocharger plays one of the most important roles in increasing the efficiency of internal combustion engines and making it more environmentally friendly.

2 Turbochargers

the turbocharger system itself, along with so many positive features, comes with a number of accompanying problems. First, from a general point of view, this device is very delicate, it needs constant maintenance, inspection, cleaning, fixing balance of the rotor and the wheels etc. In addition, during operation, turbochargers are characterized by high and rather wide frequency noise emission [27]. Such noise is mainly divided into two types: Structural bone and Air-bone noises. In both categories, we will meet some types of noise, which is caused by the structural delicacy of turbochargers and the difficulty of manufacturing them with high precision. For example, unbalanced whistle and pulsation whistle represent this type of noise. In the first case, it is caused by an unbalanced rotor,

which at the very beginning may not be made with sufficient accuracy and become even more unbalanced after a long period of operation at different speeds. Also, unbalanced rotor can create new unbalanced state, known as whip, which is quite damaging phenomena for the structure. And as for the pulsation whistle, it is caused by slight difference in compressor wheel chamber volume due to milling or moulding process variations. Apart from these, the reason for all other noises associated with turbochargers is related to the specifics of the construction of this device [1, 2].

It can be said that since the turbocharger is already an addition to internal combustion engines and with its help it was possible to obtain much higher technical data than without it without unnecessarily increasing the size of the engines, as if we have no right to be dissatisfied with this device. However, from its creation until today, it has been improved and has taken on a relatively complex look. Despite this, the multi-component construction of turbochargers can be divided into three main parts in the simplest way. These are turbine, compressor and shaft-bearing system. The turbine and compressor are connected by a shaft that is supported by bearings. The turbine rotates at the expense of exhaust gases of high temperature and pressure, and by means of a shaft it transfers these rotations to the compressor wheel. Finally, the compressor draws in atmospheric air at the expense of these revolutions and delivers it to the engine with great pressure [50]. Figure 1 shows general structure of a rotor-bearing system of a turbocharger.

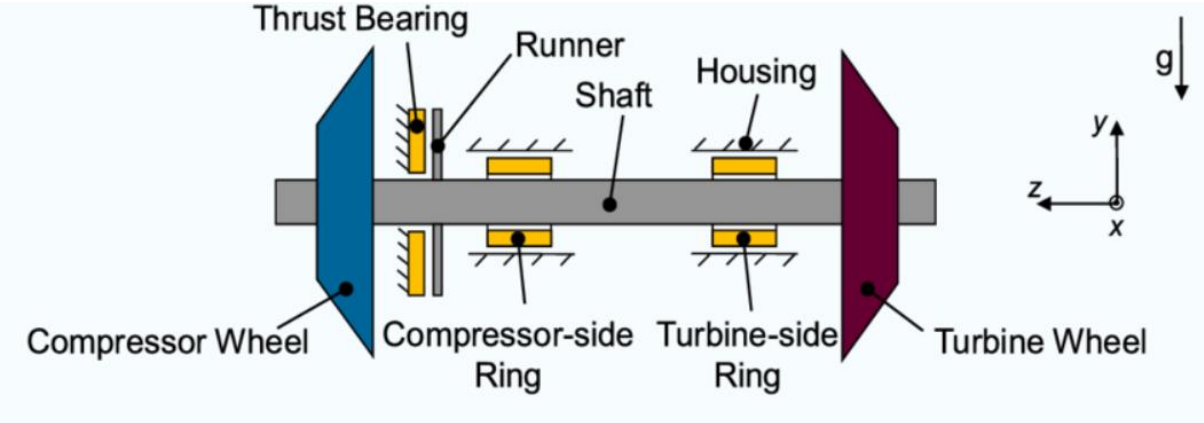

Figure 1. Schematic representation of turbocharger rotor-bearing system [6].

2.1 Short overview of several turbochargers

Nowadays, in technology, in particular in the automotive industry, we can meet the following models of turbochargers: Turbo Single, Turbo Twin, Turbo Twin-Scroll, Turbo with variable geometry, Turbo Twin Scroll variable, Electric turbo [2]. All of the above serve the same purpose, but each has its own unique side. For example, Turbo Single is distinguished from other turbochargers both by the ease of installation and the ease of construction itself.

Nevertheless, it is quite efficient and thanks to it, small displacement engines push the same power as non-turbocharged large engines. However, the Turbo Single has a narrow range of torque and this does not allow us to have high torque and peak power at the same time. Also, its response is lower or in another words turbo lag is higher compared to other turbochargers listed above [2].

2.1.1 Turbo lag

Turbo lag, to put it briefly, is the turbocharger's poor transient response at low engine loads. It is the turbocharger issue that is most commonly acknowledged. Fig. The main causes of turbocharger lag for a SI engine are depicted in figure 2. [12].

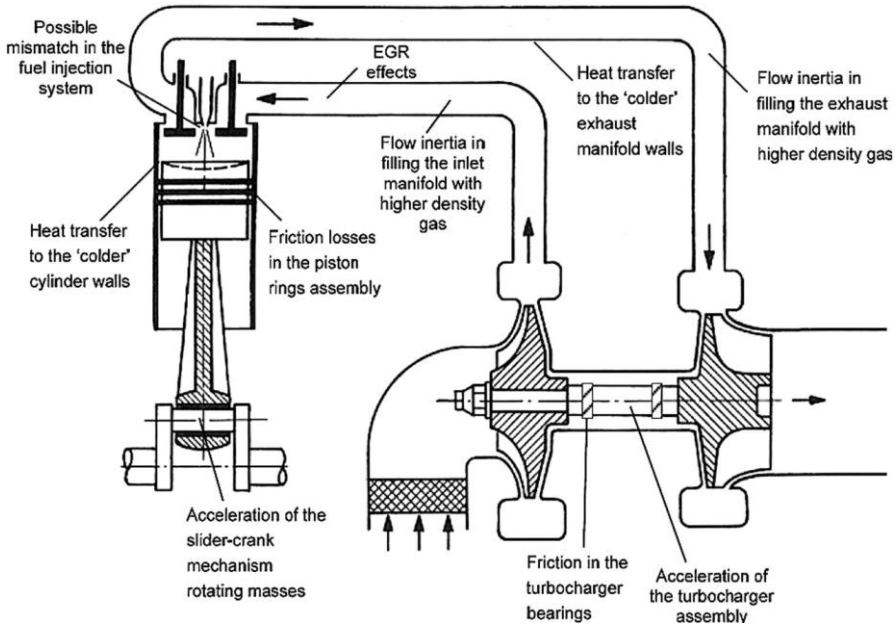

Figure 2. A demonstration of the primary cause of the system delay during a turbocharged engine's transient response [12].

As we can see one of the main causes of the turbo lag is friction in the bearings. We will show the importance of bearings in turbochargers later.

2.1.2 Influence of firing order on turbocharger performance

In addition to this it is also important to mention that the performance of turbochargers in general depends on the firing order of the engine as well. For example, we have a four-cylinder gasoline internal combustion engine and the spark supply to the combustion chambers takes place separately in a certain order, such as 1-3-4-2 (figure 3). In such a case, the subsequent reduction stage of high pressure created by the exhaust gases from the cylinders will coincide with the high-pressure pulse received from the next cylinder, and so

on. The negative side of this is that by matching the areas of high and low pressure in the exhaust gas pipe, we get a low overall pressure.

There is the following solution to this problem, according to which, as in the previous case, the pistons of the four-cylinder engine deliver the exhaust gas to the turbine in pairs, but this time the firing order for the pistons in each pair coincides with each other. Since these cylinders are paired, separated from each other, and the pistons in each pair have the firing order at the same time, the pressure drop area created by the piston moving to the bottom dead centre for refuelling does not coincide the high-pressure exhaust gas pulse anymore, and as a result, we get a stronger and more effective pulse in total each time. As an example, a representation of the pressure changes with respect to shaft angle based on Chiong MS, Rajoo S, Martinez-Botas RF, Costall AW. [43] is given in Figure 3. there we see two results: one for rotary engine and one for reciprocating engine. Curves in figure 3 correspond to two revolutions of engine output shaft.

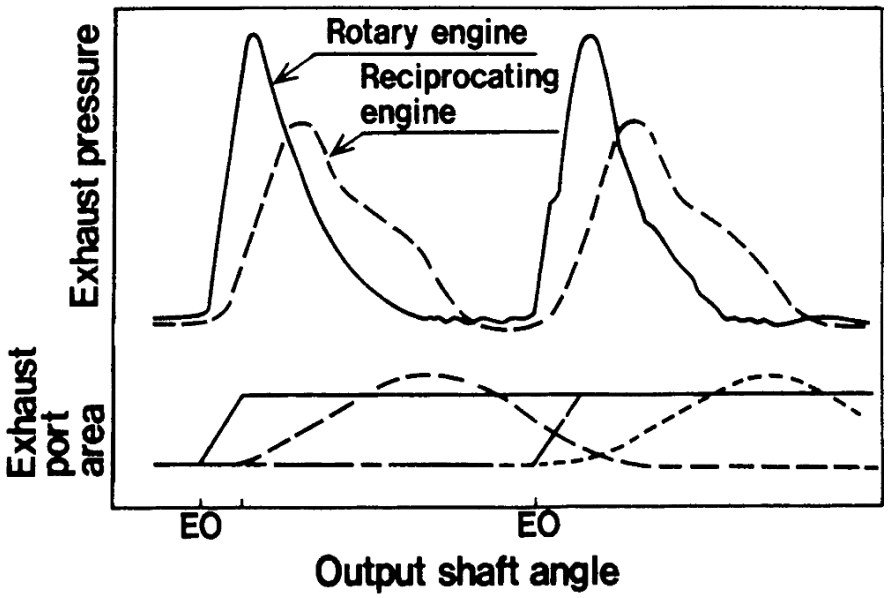

Figure 3. Exhaust pressure vs Output shaft angle [43].

The pressure change graph shown in this figure corresponds to the sequential firing order. For both types of engines, there is a sharp increase in pressure in the exhaust gas outlet pipe at the first stage, which is suitable for opening the exhaust gas valve. After that, the flow of gas in the pipe is certainly followed by several losses and the pressure starts to decrease, and finally when the fuel mixture inlet valve is opened, the pressure drops sharply on the hardening groove created by the downward movement of the piston (in the case of a reciprocating engine, for example). Finally, before opening the exhaust valve again, the pressure is equal to the atmospheric pressure indicator and the process is repeated [43].

Since for both types of engines, reciprocating engines and rotary engines, they show approximately the same behaviour with respect to the change in exhaust pressure, we will

consider one of them, for example, a reciprocating engine, and show the pressure change graphically during two different firing orders, as it was when describing the value of firing order mentioned and describe their effect on turbocharger performance. For this, if we additionally use the work of Blair GP and Goulburn JR. [3] and generalize it, then the graphs (Figure 4) will have the following shape:

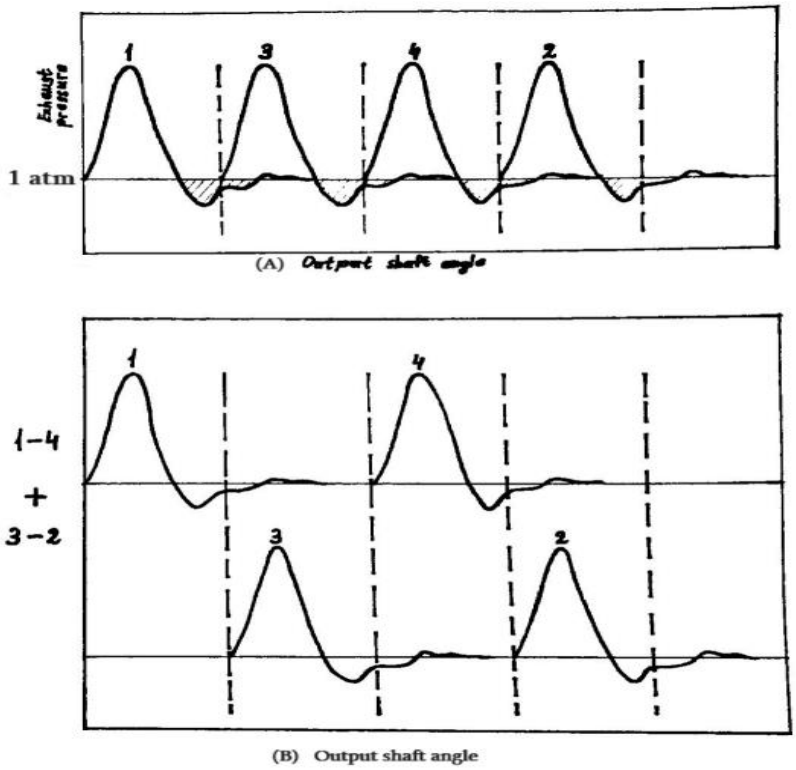

Figure 4. Exhaust pressure with respect to output shaft angle for reciprocating engines [3].

This figure directly reflects the previously mentioned discussion of the importance of firing order in turbochargers. The first part of this figure (figure 4. (A)) shows the variation of the exhaust pressure during the firing order 1-3-4-2. As we can see, as soon as the exhaust gas release valve is opened, the exhaust pressure becomes the highest value, and as in the previous picture, this pressure gradually equalizes the atmospheric pressure. However, since this drawing is simplified to show the different phases of the pressure change in reverse, and for a better visibility of the whole process in general, the vacuum conditions are clearly visible here. These are the states of the exhaust pressure when it becomes less than the atmospheric pressure due to the downward movement of the piston during the opening of the fuel gas inlet valve. These places are shown in the drawing with dashes. These are the bumpy areas that coincide with the highest value of the exhaust pressure of the second piston and cause the overall pressure to drop. This phenomenon is not observed in the bottom diagram (figure 4. (B)), where the change in exhaust pressure during the flat-twin type firing order is presented, and therefore the overall total pressure is relatively high [3].

2.1.3 twin turbochargers

As for twin turbochargers, there are two types: parallel and sequential (figure 5). In first case, two equal sized turbos are responsible for using the energy of the exhaust gas, the dimensions of which are generally noticeably smaller than what we find in the Turbo single. In sequenial tween turbocharger system there are two different sized turbos: small and large.

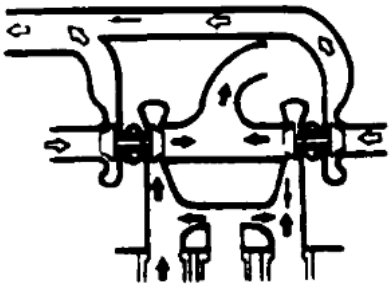

Figure 5. Sequential twin turbocharger [43].

At low engine speeds, the smaller turbo's rapid spool-up ensures smooth operation (figure 6 (A)) With the gas pedal depressed in the lower revolution range, it guarantees that the car will react quickly. The bigger turbo kicks in after the smaller turbo, delivers consistent power over a wider revolution range and gives extra boost as engine speed increases (figure 6 (B)). Twin turbos are distinguished by high performance, reduced turbo lag, wider power band than Turbo Single and better fuel economy. However, this type of turbocharger is one of the most expensive, due to its complex construction and additional details. The complexity of its system makes its maintenance even more difficult and expensive. To summarise, twin turbos are a cost and complexity-effective way to balance performance and flexibility [2].

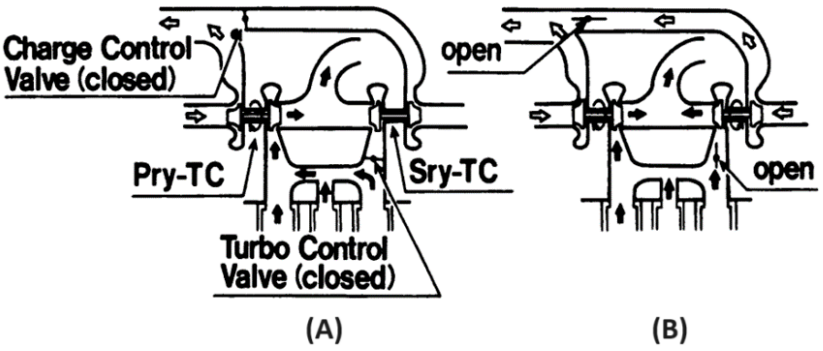

Figure 6. (A) firs sequence; (B) second sequence [43].

2.1.4 Twin-Scroll Turbocharger

Twin-Scroll Turbocharger is more or less similar to Twin-sequential turbo, because here attention is also paid to the distributed supply of exhaust gases to the turbine according to different engine revolutions, although in this case the difference is that the turbocharger itself is one and the turbine is supplied by two scrolls with bigger and smaller diameters, meaning that the exhaust gases are divided into two streams. So, for example, those two cylinders of a four-cylinder engine supply one of the scrolls (smaller diameter) by its exhaust gas, which occupy the first two places in the ignition order, and the second scroll (bigger diameter) is supplied from the other two cylinders accordingly. This result is distinguished by the fact that the cylinders connected by the principle mentioned above allow to reduce the impulses of the exhaust gas in its exhaust pipe. These pulses are caused by the collision of low-pressure, more precisely sub-atmospheric pressure gases and high-pressure airs in the same duct. Twin-Scroll Turbo eliminates exactly such cases, significantly reduces turbo lag, delivers exhaust gas to the turbines at a much higher pressure, and accordingly the compressor pumps air into the combustion chamber of the engine with more power. All this clearly indicates a more efficient and powerful operation of the engine. Twin-Scroll Turbo shares the negative sides of the previous model with the difference that here the turbocharger is characterized by low performance at high engine RPM [8, 5, 45].

2.1.5 Turbo with variable geometry (VGS)

Turbo with variable geometry is another type of turbocharger that is distinguished by its unique design. According to source [25] it skilfully uses the change in the ratio of the cross-sectional area of the exhaust gas pipe and the radius of the turbine, which it does by using additional elements - Vanes. Vanes are a kind of valves that surround the engine, and the exhaust gas passes through these valves to the turbine wheel. At low engine speeds, when there is little exhaust, these valves narrow and speed up the gas as it passes through, helping the turbine to accelerate faster. At high engine speeds, the valves expand and maintain high boost. According to the source [2] all this significantly reduces turbo lag and allows effective turbocharging at a wide RPM range. Variable geometry turbocharger is also referred to as VGT, although there are other types of turbochargers such as: Variable nozzle turbo (VNT), Variable turbine geometry (VTG), Variable geometry system (VGS), Variable turbine area (VTA). The negative side of this type of turbos is their complex construction, high cost and perishability.

2.1.6 Turbo Twin Scroll variable

As for the Turbo Twin Scroll variable, it is a kind of modification of the Twin-Scroll Turbo in that, as in its original model, there are two ducts for the exhaust gas, but now with an additional valve [45]. As mentioned earlier, the Twin-Scroll Turbo is quite an effective solution, because, to summarize, a small diameter scroll provides fast boost, and a large diameter scroll provides high power. However, at high engine speeds, a small diameter scroll is not only no longer necessary, but also creates a problem due to its back press. According to source [45] Turbo Twin Scroll variable additional valve, it can also be called shutter, serves to

solve this problem. At low engine speeds, it closes one duct and allows the exhaust gas to pass through only one scroll to the turbine, acting as the Twin-Scroll Turbo's smaller-diameter scroll equivalent. At high engine revolutions, this shutter opens gradually, and the gas can move through the second scroll, which means an increase in the diameter of the curved duct. This allows the turbocharger to operate with high flow capacity and achieve high power. Based on all this according to the source [2], the Turbo Twin Scroll variable is characterized by a wide and flat torque curve with a quick boost, is more cost effective than VGT, and it is made of such material to be able to work with high temperature exhaust gases, which are mainly found in gasoline engines.

2.1.7 Electric turbocharger

Based on the source [14] in the automotive industry, electric turbochargers, also known as e-turbos, are a cutting-edge technology that blend electric power and conventional turbocharging techniques. An intriguing option for improving engine efficiency and performance is the use of electric turbochargers. They do, however, have cost and complexity trade-offs. Conventional turbochargers, as we already know, work by using exhaust gases to turn a turbine. The turbine compresses air and forces it into the engine's combustion chamber, increasing power by burning more fuel. However, in this instance, electric turbos complement this configuration with an electric motor that can spin the compressor without relying on the exhaust flow. This means that the lag associated with conventional turbos is eliminated because the turbo can deliver an instantaneous boost when needed. When necessary, the electric motor can quickly spool up the turbo to produce instantaneous power. As a result, by helping the engine run at low RPMs, where conventional turbos might not be useful, they can increase fuel efficiency [2]. Furthermore, because electric turbos provide more precise control over the engine's air-fuel mixture, they can aid in the reduction of overall emissions. However, the turbo system becomes more complex with the addition of an electric component, which may affect maintenance costs and reliability. Also, compared to conventional turbochargers, the technology is relatively new and may be more expensive to implement. Furthermore, the vehicle's electrification is needed to power electric turbos [2].

3 Bearings in turbochargers

Bearings come in a range of shapes and sizes and are an essential tribological part of many different types of machinery. The study of interacting surfaces in relative motion is known as tribology. Bearings are a sort of machine component that restricts the types of motion they may support in a system that may be subject to static or dynamic loads. Direct contact between two metal components in relative motion is mostly avoided by bearings. By doing this, friction, heat production, and eventually part wear and tear are avoided. Due to the replacement of sliding action with low friction rolling, energy consumption is also decreased.

Additionally, they transfer the spinning element's load to the housing. This load can be either radial, axial, or both. The ability of moving parts to move freely is also restricted by a bearing [41].

The bearing system in the turbocharger mainly consists of two functionally different bearings: thrust bearings and radial bearings. The thrust bearing receives the axial loads generated in the turbocharger, while the radial bearing is responsible for the driven loads of the rotating axis. Both together ensure the mechanical stability of the entire system, and therefore their correctness is very important for the efficient operation of the whole mechanism. That is why great attention is paid to their selection. It is necessary to take into account a number of operating conditions, such as the number of revolutions of the axis and its geometric dimensions, the physical characteristics of the lubricant (oil), its incoming pressure and temperature, and many other things that we will talk about in detail later. In automotive engineering and especially in turbocharging, bearings that respond to the above-mentioned requirements (radial and axial loads) in general they are known under the following names: plain or sliding bearings and rolling element bearings. Because rolling element bearings greatly reduce bearing friction at low rotor speeds, they are occasionally used in automotive turbochargers to further improve transient behaviour or maintain low CO2 emissions in compliance with current emission laws. Because of the rising temperature of the lubricant (mostly oil), the difference in bearing friction between sliding bearings and rolling-element bearings is negligible at high rotor speeds. Consequently, the oil's viscosity decreases, which lowers the bearings' friction [26].

3.1 Sliding bearings

Sliding contact bearings are also known as simple bearings or plane bearings. A thin layer of quickly moving pressurized liquid or gas supports the load in sliding bearings, which have two bearing surfaces. Fluid bearings feature reduced friction, wear, and vibration than many other types of bearings because there is no sliding friction caused by the contact between the moving parts. Therefore, if used properly, some fluid bearings may have almost zero wear [35].

Depending on load the journal bearing supports a load in the radial direction and thrust bearing supports loads in the direction of the shaft axis. Depending on configuration there are solid bushing and split bushing. Bushing is the part of the sliding bearing which is kind of a ring surrounds a journal with a clearance filled by lubricant or any viscous fluid or gas. However, usually hydrodynamic oil-film bearings are used in the automotive turbochargers, which means that bushing in this case surrounds a journal by some specific type of oil [35].

3.1.1 Journal bearing

In case of journal bearing, we have two main parts: a shaft, so called "journal" and a hollow cylinder, in another words a "sleeve". This last one, which carries the shaft, is a bearing [38].

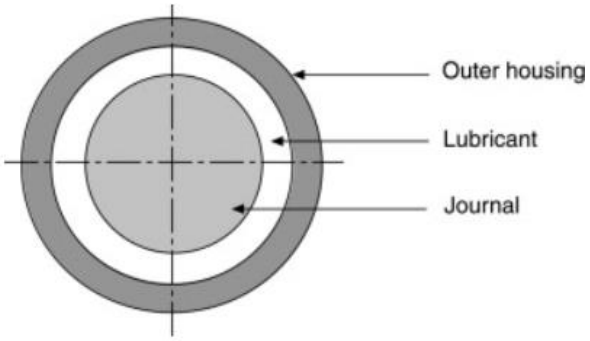

Figure 7. Basic geometry of the journal bearing [21].

Known as rotating floating ring bearings (RFRB), radial bearings rotate and float in the inner and outer oil films. In comparison to semi-floating ring bearings (SFRB), these bearings are used in automotive turbochargers to lower bearing friction, particularly at low torque. This explains why at low rotor speeds, the response behaviour of turbochargers, or turbolag, improves. The oil inlet of the bearing system receives pressurized oil for the rotating-floating ring bearing. There are two primary uses for the pressurized oil that the oil channels in the bearing housing supply: thrust and radial bearing work. In order to keep the rotor stable in both axial and radial directions and to prevent its response from large amplitude at resonance, the bearing forces produced by the oil hydrodynamic effect firstly dampen the rotor vibration. Additionally, the induced heating flow in the bearings is eliminated by the radial conduction between two oil-films through the bearing ring and the axial convection that occurs when new supply oil is introduced. By maintaining the lowest feasible effective oil temperature in the bearings, this cooling mechanism helps to maintain high rotor speeds, which in turn maintains high bearing stiffness and damping forces [26].

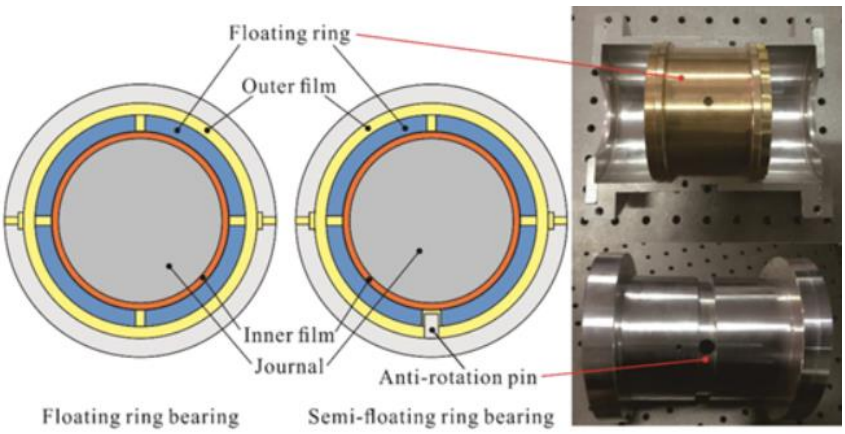

Figure 8. Typical structures of a floating ring bearing and a semi-floating ring bearing [49].

3.1.2 Thrust bearing

The thrust bearing is positioned between the thrust rings that are fixed in the shaft and rotates with the rotor; it is mounted and fixed in the bearing housing. To maintain the rotor's balance against the axial thrust, the thrust bearing's reacting force acts on one of the thrust rings. The oil-film thickness determines the thrust bearing's reacting force because the thrust bearing force is created by the oil film being squeezed between the thrust rings and the bearing. Keep in mind that the thrust bearing force is induced by a smaller oil-film thickness and vice versa [26].

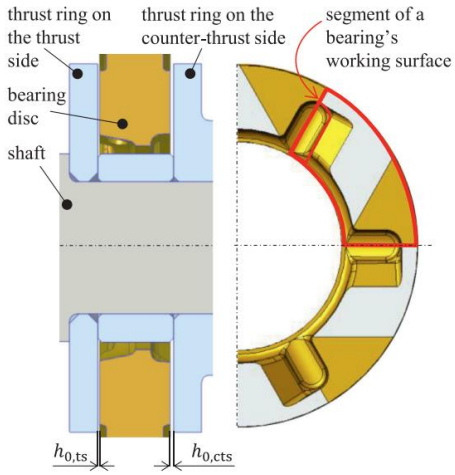

Figure 9. A cross section of the double-sided thrust bearing schematically showing the components and a segment of a bearing's working surface. The symbols $h_{0,ts}$ and $h_{0c,ts}$ indicate the minimum thickness of the lubricating gap on the thrust and counter-thrust side, respectively [29].

3.2 Stribeck graph

Sribeck graph (*figure 10.*) shows the effect of rotor speed on the coefficient of friction of the journal bearing and the thickness of the oil layer between the journal and the outer ring. Based on the initialization of a simple bearing, these curves show that a molecular lubricant layer is the only thing separating the stationary bearing shells and shaft. More hydrodynamic lubricant film is produced as the shaft rotates at a faster speed. The coefficient of friction initially decreases noticeably as a result of this. The coefficient of friction then decreases sharply as a full, continuous film forms over all bearing faces as the speed increases. Internal friction in the lubricating film increases the external friction as the speed increases. This causes the curve to pass a minimum coefficient of friction value and then increase only due to internal friction [24].

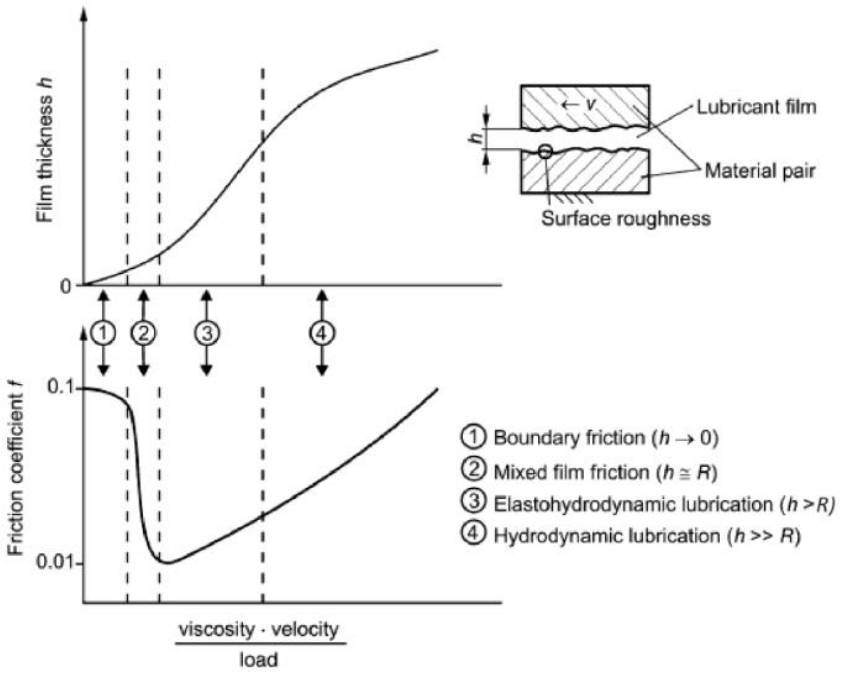

Figure 10. The Stribeck graph [24].

The four sections shown in this graphic, enclosed by dashed lines, show the state of lubrication at different rotor speeds. It would be more correct if we say that the graph shows the dependence of the type of friction or the state of lubrication on the bearing characteristic number, which is the ratio of the product of the viscosity of the oil used as a lubricant and the number of revolutions of the rotor to the so-called hydrodynamic pressure generated in the area of oil friction, which in turn is caused by the rotation of the rotor. In addition to the speed of the rotor, the emergence of these other two parameters is important because they change their value along with the change in the number of revolutions, and precisely because their change leads to a change in the state of lubrication and, accordingly, the numerical value of friction [24].

3.2.1 Boundary friction

If we look at the first section of the lower graph in Figure 10, which is referred to as boundary friction, we will notice that here the friction coefficient reaches the highest values compared to other sections presented on the graph. This is due to the fact that at low rotor speeds, the hydrodynamic pressure, which is represented in the denominator of the horizontal axis, cannot be generated sufficiently, and therefore the lifting force, which must act on the journal, is low. Due to this, the journal and bearing surfaces touch each other and we have metal-to-metal friction. The heat generated by this friction raises the temperature of the oil and thus reduces the viscosity of the lubricant. The latter phenomenon, the increase in temperature, naturally reduces the internal friction between the oil layers. However, from a mathematical point of view, by reducing the number of revolutions of the rotor, the value of viscosity increases more than that of pressure, so the value of the bearing characteristic also

decreases, and according to the graph, this means an increase in the coefficient of friction on the vertical axis in the first and second sections. The ability for surface asperities to interact and quickly wear makes boundary lubrication less attractive than the other forms. A lot of empirical design goes into this kind of lubricant. Boundary lubrication bearings include, for example, those found in electric motor shafts, office equipment, power screw support bearings, and electric fan bearings [18].

3.2.2 Mixed lubrication

As for mixed lubrication, in this section the journal has relatively high rotation numbers, therefore, we have higher pressure and metal-to-metal friction is also reduced, although it is partially present. Due to the reduction of friction between metal surfaces, the temperature of the oil is also relatively small compared to the previous case, which leads to an increase in the viscosity of the oil and, accordingly, the bearing characteristics. The lowest friction coefficient is located on the boundary line of this section and elastohydrodynamic lubrication. Mixed lubrication state may also exist in the presence of insufficient lubrication, low viscosity, overloaded bearings, tight clearances, slow bearing speeds, and misaligned bearing assemblies [18].

3.2.3 Elastohydrodynamic lubrication

In the case of elastohydrodynamic lubrication, there is an increase in the coefficient of friction again, because here, despite the absence of friction between the surfaces of the journal and bearing walls, we still have friction, although in this case both between the oil and the rotating metal surfaces, as well as between the inner layers of the oil itself. All this, of course, is due to the increased viscosity at the expense of the low temperature of the lubricant. Also, the relationship between the elastic deformation of the supporting materials and the hydrodynamic action of full-fluid films is the subject of elastohydrodynamic lubrication. As with mating gears and rolling bearings, it happens when lubricant is injected between surfaces that are in rolling contact [35].

3.2.4 Hydrodynamic lubrication

The hydrodynamic friction region is the lubrication condition that can be said to be the most desirable for sliding bearings in automatic turbochargers. There, the fluid is drawn onto the inner surface of the bearing by the bearing movement, creating a lubricating wedge beneath or around the shaft. Hydrodynamic lubrication, like its predecessor, is in the stable part of the bearing operation. It is called stable for the reason that, if we look at figure 10, the change in the number of revolutions of the journal does not cause a drastic increase or decrease in the friction coefficient, which cannot be said about bounder and mixed lubrication. That is why the first two lubrication states are called the unstable region [35].

3.3 Rolling element bearings

Rolling element bearings can be presented with two main types: Ball bearings and Roller bearings. Balls are used in ball bearings. Point contact between the balls and the

raceways defines them. Ball bearings often rotate quite fast but are incapable of carrying heavy loads. Deep-Groove Ball Bearings are those what generally are utilized the most comparing to other types of rolling bearings. They are employed in a variety of applications because of their straightforward design, ease of maintenance, and resistance to operating conditions. They also deflect axial forces in both directions in addition to radial forces. Additionally, its low torque qualifies them for use at greater speeds. Contact angle serves to identify angular contact ball bearings. This indicates that forces are transmitted at a specific angle from one raceway to the other. Therefore, angular-contact ball bearings are appropriate for mixed loads where large axial forces as well as radial forces must be conveyed. Self-Aligning Ball Bearings contain a continuous spherical outer ring racetrack that enables the inner ring/ball complement to revolve within the outer ring in addition to a double row of balls led by a cage and a double row inner ring raceway. This is what makes it possible for the application to self-align to some extent. When there is a difficulty with the housing and shaft alignment (misalignment), this type of bearing is advised since the shaft may deflect. The best bearings for absorbing radial forces are self-aligning ball bearings. Two bearing discs with ball raceways make up thrust ball bearings. Thrust ball bearings may position the shaft axially in one direction since they were created specifically for absorbing axial stresses in one direction [11].

Line contact is a feature of roller bearings. Due to the greater friction of a contact line, line contact has a higher load rating than ball bearings of the same size but has a lower speed capability. With the difference that they use spherical rollers rather than ball rollers, Spherical Roller Bearings are exceptionally durable and operate on the same principles as Self-aligning Bearings. This enables them to sustain higher loads. Misalignments between the shaft and the housing may be corrected by doing this. High radial and mild axial loads can be absorbed by spherical roller bearings. Line contact between the rolling components and the raceways in cylindrical roller bearings improves the distribution of stress factors at the point of contact. Because of this configuration, cylindrical roller bearings have an extremely high radial load rating. They could also be able to transfer a small number of axial loads, depending on the design. Conical rollers are placed between the inner and outer tapered raceways of tapered roller bearings, which feature tapered raceways in the inner and outer rings. High radial and axial forces may be absorbed in one direction by tapered roller bearings because of the contact angle. To sustain axial stresses in both directions, tapered roller bearings are often used in pairs. A unique variety of cylindrical roller bearings called needle roller bearings contain long, thin rolling elements called needle rollers. Between 1:3 and 1:10 applies to the diameter to length ratio. Only radial forces may be accommodated by needle roller bearings, which have a high load rating. Needle bearings may be an excellent choice if space is limited [16].

However, in the end, it should be noted that despite the many benefits of rolling element bearings, as usual sliding bearings are used in turbochargers. Especially Floating ring journal bearings are a common component of turbochargers of automobile size. Since they are more expensive initially, have a shorter lifespan, and are more difficult to replace, ball

bearings are not utilized in most commercial engine applications. Contemporary designs incorporate ceramic ball elements, and specific high-performance engines for automotive racing applications can afford the additional cost of ball bearings [1].

4 Exploring the motivation of the research

As we have already seen, bearings play an important role in rotating machines, whether it is a turbocharger or another type of mechanism. The quality of the bearings has a great influence on the efficiency of the whole mechanism, because it is a kind of conductor of mechanical energy, the main purpose of which is that this energy passes through it with as little losses as possible. Its effectiveness depends on many things. When selecting a bearing, many operational circumstances must be considered, so that under the given conditions, the mechanism of which this bearing is a part will reveal its maximum potential. To achieve this goal, we need to reduce the mechanical losses in machines, the largest part of which comes from friction in bearings in rotating machines [10]. Also Feneley AJ, Pesiridis A and Andwari AM. [12] in their paper note that friction in the bearing system is one of the causes of turbo lag. This is clearly shown in figure 2. Tashima S, Taqdokoro T, Tadokoro T, Okimoto H and Niwa Y. [43] also mention that one of the important ways to correct turbolag and low torque is to introduce variable geometry turbochargers in cars and reduce the moment of inertia (mass) of the rotor, as well as elimination of losses caused by friction in bearings. Along with this, according to the work of Deligant M, Podevin P and Descombes G.[10], in the experiments conducted to reveal the mechanical friction losses on the turbocharger, it is clearly seen that the friction in the bearing system plays a rather large role in terms of energy losses and, therefore, the drop in efficiency of the entire turbocharger mechanism. Of course, in the same work, attention is also focused on other components of the turbocharger, such as the turbine and the compressor, although the final results show that up to 80% of the total mechanical losses of the turbocharger come from the bearing system. A graphical representation of this is presented in Figure 11.

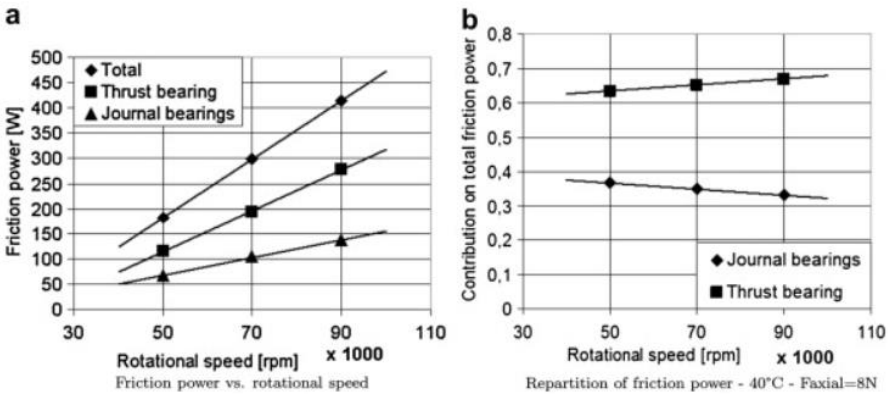

Figure 11. Friction loses of thrust and journal bearings at different rotational speeds in single scroll turbocharger [10].

"Figure 11 A" illustrates the details of friction power versus rotational speed after the friction power of bearings was calculated using experimental results from total friction

measurements with an axial force of 8 N and an oil inlet temperature of 40 °C. The thrust and journal bearing contributions to the overall friction losses are shown evolving with rotational speed in "Figure 11 B.". According to the graph, over 60% of the friction losses are attributed to the thrust bearing, which increases with increasing speed. When the speed increases, the contribution of journal bearings to the total friction loss decreases to 20% [10].

Taking all of this into consideration, there is no doubt that the friction generated in the bearing system is one of the biggest problems for the efficient operation of turbochargers. The advantage of the smooth and efficient operation of this device is again that the more efficient the turbocharger, the more it reduces fuel consumption in vehicles and other types of machines with internal combustion engines. Fuel economy itself leads to a reduction in environmental pollution caused by fuel combustion. Accordingly, with all the above in mind, my goal in this paper is to reduce friction in the turbocharger bearing system, and more specifically in the journal bearings.

5 Hydrodynamic bearing models

Hydrodynamic journal bearings are essential components in many mechanical systems, providing support and reducing friction between rotating shafts and their housings. These bearings operate by maintaining a thin film of lubricant between the bearing surface and the journal, the part of the shaft that rotates within the bearing. The lubricating film is crucial because it creates pressure that supports the load and minimizes direct contact between surfaces, reducing wear and extending the life of the machine. To accurately predict the performance of hydrodynamic bearings, various models have been developed. These models help engineers understand the complex interactions within the bearing, such as fluid dynamics, pressure distribution and material deformation. The most well-known models include the Reynolds equation [38], computational fluid dynamics (CFD) models and elasto-hydrodynamics models (EHD). The Reynolds equation is a fundamental tool in the study of hydrodynamic lubrication. It provides a simplified yet powerful means of describing the pressure distribution in the lubricating film. This equation is derived from the Navier-Stokes equations assuming thin film lubrication, making it a cornerstone in bearing performance analysis [38]. CFD models take the analysis a step further by solving the Navier-Stokes equations directly. These models provide a detailed simulation of fluid flow within the bearing and take complex geometries into account. CFD models are particularly useful for studying the dynamic behaviour of bearings and predicting performance under different scenarios. EHD models extend hydrodynamic theory by incorporating elastic deformation of bearing surfaces. This is critical in load applications where the pressure in the lubricating film can cause significant deformation of the bearing material. By combining the Reynolds equation with elasticity equations, EHD models provide a more accurate representation of bearing behaviour under real operating conditions. Together, these models provide a

comprehensive toolkit for engineers to design and optimize hydrodynamic bearings, ensuring reliable and efficient operation across a wide range of applications. Now let's take a closer look at each of these models.

5.1 Reynolds equation

By describing how a viscous liquid film forms between the moving surfaces, Reynolds' theory clarifies the lubrication mechanism. The prerequisite for creating such a film is that the surfaces must move sufficiently quickly in relation to one another. Many researchers after Reynolds discovered that the majority of oil's lubricating properties could be attributed to its relatively high viscosity. The "Reynolds equation," which was first derived by Reynolds and is widely referred to in the literature, is a mathematical expression that can be used to express all hydrodynamic lubrication. One can derive this equation in a few different ways. The equation for momentum and continuity in Navier-Stokes can be simplified and therefore derived from this basis. ON the other hand, it is often derived by considering that liquid element is at equilibrium which is subjected to viscous shear and then applying the continuity-of-flow principle. In order for hydrodynamic lubrication to occur, two requirements must be met: first, two surfaces must move relative to one another quickly enough to create a lubricating film that carries a load; second, surfaces must be angled, in another words, if the surfaces are parallel, the lubricating film will not develop a pressure field strong enough to sustain the necessary load. A schematic representation of the hydrodynamic pressure generation principle between moving non-parallel surfaces can be found in Figure 12. [38].

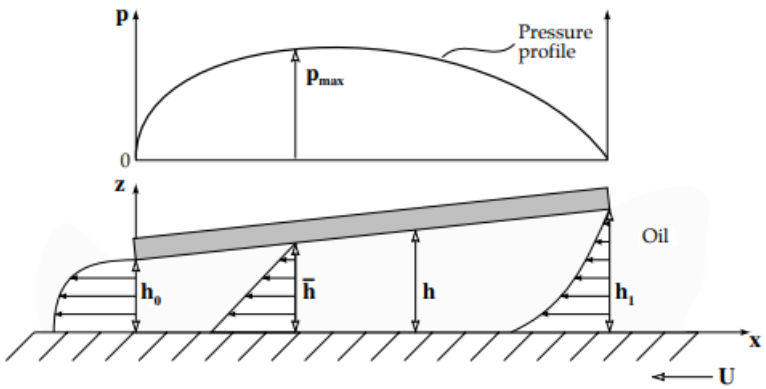

Figure 12. Principle of hydrodynamic pressure generation between non-parallel surfaces [38].

It is likely that the lower surface, sometimes referred to as the "runner," is lubricant-coated and moves at a specific speed. A specific angle separates the top and bottom surfaces. The lubricant is drawn into the converging wedge by the bottom surface as it moves. Because there would be more lubricant entering the wedge than exiting it, a pressure field is created. As a result, as the wedge begins, rising pressure limits the entry flow, and falling pressure at the exit increases the exit flow. As a result, as illustrated in Figure 12, the fluid

velocity profile bends inward at the wedge's entrance and outward at its exit due to the pressure gradient. In addition to separating the two surfaces, the generated pressure can bear a specific weight. To create a journal bearing, the wedge can also be bent or wrapped around a shaft. A pad bearing is produced if the wedge stays planar. It is possible to accurately predict bearing characteristics by providing a mathematical description of the entire process of hydrodynamic pressure generation [38].

Exact mathematical equations cannot adequately describe the controlling processes in the majority of engineering applications due to their complexity. A description like this would be nearly impossible due to the numerous variables and interacting factors present in the real processes. As an illustration, internal fluid friction terms were disregarded in the early days of fluid mechanics modeling. With the advent of computers, the landscape drastically shifted, allowing for a more thorough examination of mechanical systems. A mathematical description of the basic underlying mechanisms in hydrodynamics cannot be derived without first making a number of simplifying approximations. Following this, it is convenient to derive the Reynolds equation by taking into account the continuity of flow in a column and the equilibrium of an element, from which the expressions for fluid velocities can be obtained [38]. These examples are shown in table 1.

Table 1. An overview of hydrodynamics' simplifying assumptions [38].

	Assumption	Comments
1	Body forces are neglected	Always valid, since there are no extra outside fields of forces acting on the fluids with an exception of magnetohydrodynamic fluids and their applications.
2	Pressure is constant through the film	Always valid, since the thickness of hydrodynamic films is in the range of several micrometers. There might be some exceptions, however, with elastic films.
3	No slip at the boundaries	Always valid, since the velocity of the oil layer adjacent to the boundary is the same as that of the boundary.
4	Lubricant behaves as a Newtonian fluid	Usually valid with certain exceptions, e.g., polymeric oils.
5	Flow is laminar	Usually valid, except large bearings, e.g., turbines.
6	Fluid inertia is neglected	Valid for low bearing speeds or high loads. Inertia effects are included in more exact analyses.
7	Fluid density is constant	Usually valid for fluids when there is not much thermal expansion. Definitely not valid for gases.
8	Viscosity is constant throughout the generated fluid film	Crude assumption but necessary to simplify the calculations, although it is not true. Viscosity is not constant throughout the generated film.

5.1.1 Equilibrium of fluid element

According to teh source [38] to derive the Reynolds equation, as mentioned above, it is necessary to first write the element equilibrium equation.derivation is from the source [38]. There is ment that the forces on this element initially act only on the x-axis. If this point is in

equilibrium on this axis, which means that the forces from the left and the right balance each other, then we have :

$$(1)\quad pdydz + \left(\tau_x + \frac{\partial \tau_x}{\partial z} dz\right) dxdy = \left(p + \frac{\partial p}{\partial x} dx\right) dydz + \tau_x dxdy$$

Where, p is the pressure and τ_x is the shear stress on x axis. Graphical representation of a fluid element and forces acting on it is shown in figure 13.

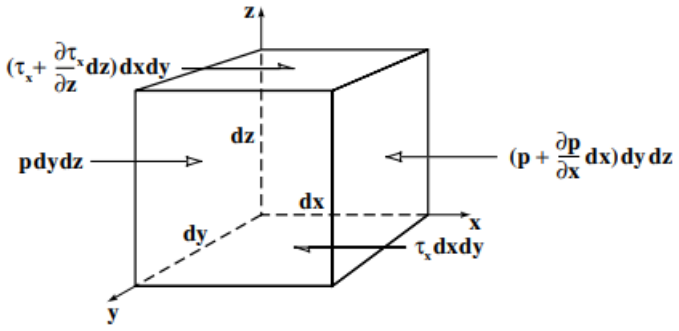

Figure 13. Equilibrium of an element of fluid from a hydrodynamic film [38].

Considering that $dxdydz \neq 0$ and we divide both sides on it we get this for x axis $\frac{\partial \tau_x}{\partial z} = \frac{\partial p}{\partial x}$ (2) and this for y axis (3) $\frac{\partial \tau_y}{\partial z} = \frac{\partial p}{\partial y}$ which is second equilibrium condition. According to second assumption mentioned above, there is no pressure difference on z axis $\frac{\partial p}{\partial z} = 0$.

By accounting u and v as the velocities on the x and y axes respectively, also h as the film thickness, expressing τ_x and τ_y with dynamic viscosity η according to the source [39] will have this face:

$$(4)\ \tau_x = \eta \frac{u}{h} = \eta \frac{du}{dz} \quad and\ (5)\ \tau_y = \eta \frac{v}{h} = \eta \frac{dv}{dz}.$$

To proceed derivation from the source [38], by substituting them back to (2) and (3):

$$(6)\ \frac{\partial p}{\partial x} = \frac{\partial}{\partial z}\left(\eta \frac{du}{dz}\right) \quad \text{and } (7)\ \frac{\partial p}{\partial y} = \frac{\partial}{\partial z}\left(\eta \frac{dv}{dz}\right).$$

Assumption 8 helps us easily integrate (6) and (7) twice since η is nor a function of z, however for now all of the actions will be made for y axis and then in a seimilar manner we can obtain the result for y axis : (8) $\frac{\partial p}{\partial x} \frac{z^2}{2} + C_1 z + C_2 = \eta u$

Assuming the third assumption the boundary conditions will be:

$u = U_2$ when $z = 0$ and $u = U_1$ when $z = h$.

Using this boundary conditions C_1 and C_2 can be calculated:

$$C_2 = \eta U_2 \quad \text{and} \quad C_1 = (U_1 - U_2)\frac{\eta}{h} - \frac{\partial p}{\partial x}\frac{h}{2}.$$

Now if we substitute these in (8) and simplify it finally gets analytical expression of velocity on x axis:

$$(9)\quad u = \left(\frac{z^2 - zh}{2\eta}\right)\frac{\partial p}{\partial x} + (U_1 - U_2)\frac{z}{h} + U_2.$$

Similarly, for y axis:

$$(10)\quad v = \left(\frac{z^2 - zh}{2\eta}\right)\frac{\partial p}{\partial y} + (V_1 - V_2)\frac{z}{h} + V_2.$$

Schematic representation for both types of velocities due to these three separated terms including in formulas are the same and shown in figure 14.

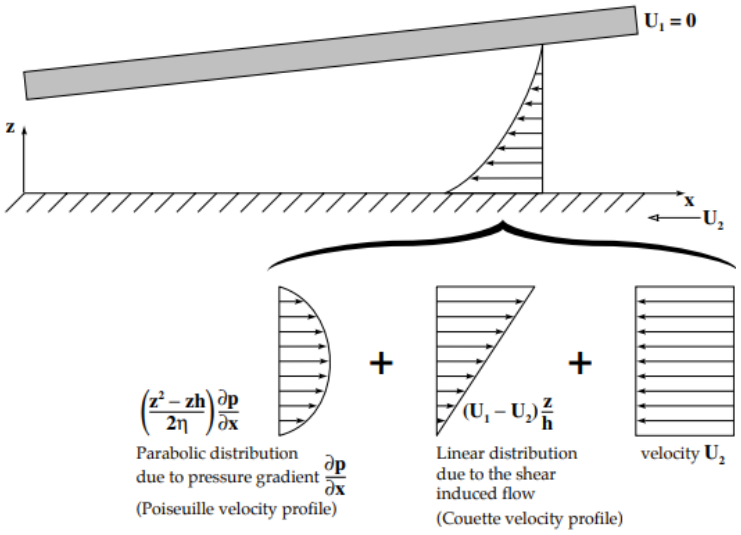

Figure 14. Velocity profiles at the entry of the hydrodynamic film [38].

5.1.2 Applying flow continuity in a column

According to the source [38] in a steady state, a liquid's influx and outflow from a control volume must be equal according to the continuity of flow principle. If the assumption 7 will be considered as well, then we have:

$$(11)\quad q_x dy + q_y dx + w_0 dx dy = \left(q_x + \frac{\partial q_x}{\partial x}dx\right)dy + \left(q_y + \frac{\partial q_y}{\partial y}dy\right)dx + w_h dx dy.$$

Where q_x, q_y and $w_0 dxdy$ represents inflow in the column. $q_x + \frac{\partial q_x}{\partial x} dx$, $q_y + \frac{\partial q_y}{\partial y} dy$ and $w_h dxdy$ shows Outflows. w_0 and w_h are up-moving speeds of bottom and top of the column respectively. Schematically it is shown in figure 15.

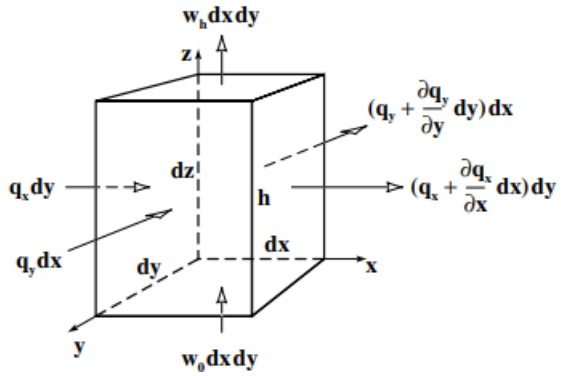

Figure 15. Continuity of flow in a column [38].

Considering that $d_x d_y \neq 0$ farther simplification gives us flow continuity equation in column:

$$(12)\quad \frac{\partial q_x}{\partial x} + \frac{\partial q_y}{\partial y} + (w_h - w_0) = 0.$$

Integration of the lubricant velocity profile over the film thickness yields the flow rates per unit length, or q_x and q_y:

$$(13)\quad q_x = \int_0^h u dz = -\frac{h^3}{12\eta}\frac{\partial p}{\partial x} + (U_1 + U_2)\frac{h}{2}$$ the flow rate in the x direction

And

$$(14)\quad q_y = \int_0^h v dz = -\frac{h^3}{12\eta}\frac{\partial p}{\partial y} + (V_1 + V_2)\frac{h}{2}$$ the flow rate in the y direction.

Substitute (13) and (14) back to (12). Also, determine that $U = U_1 + U_2$, $V = V_1 + V_2$, $U \neq f(x)$ and $V \neq f(y)$, then we get the full Reynolds equation in three dimensions:

$$(15)\quad \frac{\partial}{\partial x}\left(\frac{h^3}{\eta}\frac{\partial p}{\partial x}\right) + \frac{\partial}{\partial y}\left(\frac{h^3}{\eta}\frac{\partial p}{\partial y}\right) = 6\left(U\frac{\partial h}{\partial x} + V\frac{\partial h}{\partial y}\right) + 12(w_h - w_0).$$

On the other hand, this form of Raynolds equation is quite complicated and as usual, it is not used to be seen in engineering applications. To make it valid for practical use it requires several simplifications, such as choosing axes so that one of the velocities equals zero. For example, for journal bearings it is extremely rare that bearing slides along the shaft, so an assumption $V = 0$ is quite helpful for this kind of applications [38]. In addition to this, vertical flow is also used to be taken out from the equation. However asssuming that fluid

surfaces always maintain distance between sliding layers, in another words $(w_h - w_0) = 0$, is not too much close to the reality. whether it is possible to reduce bearing vibrations during the operation or even more, completely damp and vanish it, and on top of that exclude porosity in the bearings, mixing of fluid layers would be avoided. However, it is also quite far from the truth [38].

Nevertheless, according to the [38] it still is a common practice to assume that there is no vertical flow. Next assumption is to apply isoviscosity in the equation, which means that $\eta = \text{const}$. this approach is also very common in various engineering applications. Taking all this into account, the Reynolds equation will be written in this form:

$$(16) \quad \frac{\partial}{\partial x}\left(h^3 \frac{\partial p}{\partial x}\right) + \frac{\partial}{\partial y}\left(h^3 \frac{\partial p}{\partial y}\right) = 6U\eta \frac{\partial h}{\partial x}.$$

This is the most used form of Reynold's equation for the journal bearing applications.

5.1.3 Long and short bearing theories

Despite such simplification of the Reynolds equation, it cannot be solved analytically, since it is two-dimensional and therefore requires a numerical solution. However, based on the source [38], where farther derivations will be taken from, it turns out that there are ways to simplify the Reynolds equation even more, and they are known as the long bearing and short bearing theories. According to the first theory, it is possible to imply that the pressure gradient along the y-axis is much smaller than along the x-axis, in other words $\partial p/\partial y = 0$. This allows the Reynolds equation to be reduced to one dimension, which allows its analytical solution. According to the long bearing theory, the second term on the left side of the Reynolds equation becomes zero, and the equation takes the following form:

$$(17) \quad \frac{d}{dx}\left(h^3 \frac{dp}{dx}\right) = 6U\eta \frac{dh}{dx}.$$

As for the short bearing theory, here the issue is the opposite. This means that when the ratio of the length of the bearing to the inner diameter is less than one third (d/b < 1/3), then it becomes possible to exclude the first term from the equation due to its much lower value compared to the second term, that is, to mean that $\partial p/\partial x = 0$. According to the short bearing theory, the Reynolds equation looks like:

$$(18) \quad \frac{d}{dy}\left(h^3 \frac{dp}{dy}\right) = 6U\eta \frac{dh}{dx}.$$

5.2 CFD model

In recent years, three-dimensional computational fluid dynamics (3D CFD) has emerged as a powerful tool for simulating and analyzing the behavior of journal bearings in turbochargers. CFD is a branch of fluid mechanics that uses numerical methods and algorithms to solve and analyze problems involving fluid flows. By solving the Navier-Stokes equations, which describe the motion of fluid substances, CFD provides detailed

insights into the flow characteristics within complex geometries. In the context of journal bearings, 3D CFD models can simulate the intricate interactions between the lubricant, bearing surfaces, and the rotating shaft, offering a comprehensive understanding of the lubrication dynamics [37].

5.2.1 Geometry and meshing

The first step in developing a 3D CFD model for a turbocharger journal bearing involves creating a detailed geometric representation of the bearing assembly. This includes the shaft, bearing sleeve, and the lubrication film. The clearance between the shaft and the sleeve, typically in the micrometer range, must be accurately modeled to capture the thin lubrication film's behavior. As for the meshing, meshing the geometry involves dividing it into small, discrete elements or cells, where the fluid flow equations will be solved. The quality of the mesh is crucial for the accuracy of the simulation. A fine mesh is required in the lubrication film region to resolve the thin film's flow characteristics accurately. However, a balance must be struck between mesh density and computational cost [17].

5.2.2 Governing equations and boundary conditions

The core of the CFD model is the set of governing equations, primarily the Navier-Stokes equations, which describe the conservation of mass, momentum, and energy within the fluid. These equations are solved numerically within the bearing domain to predict the lubricant's pressure, velocity, and temperature distributions. Aslo, appropriate boundary conditions are essential for realistic simulations. Common boundary conditions for journal bearing simulations include: inlet outlet and wall boundary conditions. First of them is nessesary to specify the lubricant's flow rate or pressure entering the bearing clearance. The second is to define the pressure or flow rate at which the lubricant exits the bearing and the last one is to Represent the interactions between the lubricant and the bearing surfaces, typically assuming no-slip conditions (zero velocity at the wall). As for the lubricant's properties, they significantly influence the bearing's performance. These properties, including viscosity, density, and thermal conductivity, can vary with temperature and pressure. Incorporating temperature-dependent viscosity models is essential to capture the lubricant's behavior accurately under varying thermal conditions within the bearing [17].

5.2.3 Simulation and analysis

Once the CFD model is set up with the appropriate geometry, mesh, boundary conditions, and lubricant properties, the simulation can be performed. The solver iteratively calculates the flow variables until convergence is achieved, where the changes between successive iterations fall below a specified threshold. The simulation results provide detailed insights into the lubricant film's pressure distribution, velocity profiles, and temperature fields. Key performance metrics for the bearing, such as load-carrying capacity, frictional losses, and film thickness, can be extracted from the simulation data [37].

5.2.4 Challenges

Despite the advances in 3D CFD modeling, several challenges remain. High-fidelity simulations require significant computational resources and time, especially for transient analyses involving dynamic loading conditions. Developing efficient algorithms and leveraging high-performance computing (HPC) resources are essential for practical applications. Another challenge is accurately modeling the lubricant's rheological properties, especially under extreme conditions. Experimental data and advanced material models are needed to capture the non-Newtonian behavior of lubricants accurately [37].

5.3 EHD model

The Elastohydrodynamic (EHD) model is an essential tool for analysing and optimizing journal bearings under high-load, high-speed conditions. By accounting for both the fluid film lubrication and the elastic deformation of the bearing surfaces, the EHD model provides a quite accurate and comprehensive prediction of bearing performance. While the model's complexity and computational requirements pose challenges, its benefits in terms of accuracy and applicability make it invaluable for the design and analysis of journal bearings in demanding applications such as turbochargers, automotive engines, and industrial machinery [53].

Implementing the EHD model for journal bearings involves several steps, each crucial for accurately capturing the complex interactions between the lubricant and the bearing surfaces. The first step is to define the geometry of the journal bearing and the operating conditions. This includes specifying the dimensions of the bearing and shaft, the type of lubricant, rotational speed, and applied load. The accuracy of these inputs is critical, as they directly influence the simulation results [52]. On top of that, material properties of the bearing and shaft, such as Young's modulus and Poisson's ratio, must be specified. These properties are essential for calculating the elastic deformation of the surfaces The lubricant's pressure-viscosity relationship also needs to be defined, as it influences the pressure distribution and film thickness [7]. Also, the bearing domain is discretized into a grid or mesh, depending on the chosen numerical method. The grid resolution must be fine enough to capture the variations in pressure, film thickness, and deformation, especially near the edges of the contact area where these quantities can change rapidly [51]. For the next step the coupled Reynolds equation, elasticity equation, and film thickness equation are solved iteratively. An initial guess for the pressure distribution and film thickness is made, and the equations are solved using the chosen numerical method. The results are then used to update the film thickness and pressure distribution, and the process is repeated until convergence is achieved [23]. And finally, once the solution converges, the results are analysed to assess the performance of the journal bearing. Key outputs include the pressure distribution, film thickness, and surface deformation. These results can be used to evaluate the load-carrying

capacity of the bearing, the risk of metal-to-metal contact, and the overall lubrication performance under the specified operating conditions [48].

5.3.1 Advantages and Challenges of the EHD Model

The EHD model provides a more accurate prediction of lubrication performance under high-load conditions by accounting for elastic deformation of the bearing surfaces. Also, by integrating fluid film lubrication with elasticity theory, the EHD model offers a comprehensive analysis of bearing performance, including pressure distribution, film thickness, and surface deformation. In addition to this, the EHD model is applicable to a wide range of high-load, high-speed applications, making it a versatile tool for bearing design and analysis [15].

As for the challenges, the EHD model is quite complex, requiring the solution of coupled nonlinear equations. This complexity increases the computational effort and time required for analysis. Also, the need for fine grid resolution and iterative solution methods means that the EHD model can be computationally expensive, especially for large-scale problems. And on top of that, Accurate implementation of the EHD model requires detailed material properties, lubricant characteristics, and operating conditions, which may not always be readily available [15].

6 A review of existing research

The above models represent the methods of determining many parameters of the processes taking place in the bearings. The results obtained in the process do not serve only for the technical accounting of the process. It can be said that the main reason for conducting each report is to use the obtained information to improve the object of observation, in our case Journal Bearing. It can be improved in many ways, and it certainly depends on the application, but as I mentioned before, my main goal in the journal bearing is to reduce friction. A lot of research and work has been done on this issue. Let's consider some of them.

6.1 Research N1

One of the interesting visions in optimisation of journal bearing is suggested form Ali Usman and Ceol Woo Park [44], who employed a hydrodynamic lubrication model to assess the impact of surface textures on journal bearing performance under varying operating conditions in their study - “Numerical optimization of surface texture for improved tribological performance of journal bearing at varying operating conditions”.

In the study by Usman A and Park CW [44], the authors employed a hydrodynamic lubrication model to assess the impact of surface textures on journal bearing performance under varying operating conditions. The model used the two-dimensional generalized

Reynolds equation coupled with a mass-conserving Elrod cavitation algorithm to simulate the effect of texture-induced variations on tribological performance parameters. Key geometrical parameters considered in the study [44] include texture area density and aspect ratio. These dimensionless parameters describe the distribution and shape of the surface textures. The authors opted for a 50% area density and a partially textured surface, covering 60% of the bearing's length, as these configurations were shown to be effective in previous studies.

The study [44] treats surface textures as global variations in the lubricating film, which in turn affects the distribution of the lubricating oil film in the bearing. The Reynolds equation, which is widely used to calculate hydrodynamic pressure in lubricated interfaces, was modified to account for the presence of surface textures and cavitation where the lubricant film breaks down into a mixture of liquid and vapor. The authors [44] also considered boundary conditions where gauge pressure is used as the reference, and a symmetric boundary condition is applied at the half-width of the bearing to reduce computational load. The load-carrying capacity, a critical performance parameter, was calculated by integrating the hydrodynamic pressures over the journal surface.

The study [44] employed the finite element method (FEM) via the COMSOL software to solve the governing equations. COMSOL was chosen for its ability to handle complex, non-linear equations and its flexibility in defining custom boundary conditions and material properties. The Newton–Raphson method was used for iterative convergence, and a mesh dependency test was conducted to ensure accuracy, with mesh B being selected for its balance between accuracy and computational efficiency. A series of over 300 simulations were conducted to explore the effects of various groove geometries on friction and load-carrying capacity. The optimization process focused on reducing frictional response while maintaining load-carrying capacity, considering different speeds and loads to understand the influence of operating conditions on tribological performance.

The results of [44] demonstrated that surface texturing could significantly reduce friction in journal bearings. Transverse grooves, in particular, were effective in reducing friction due to their ability to disrupt the lubricating film, creating localized micro-hydrodynamic effects that lower resistance to sliding. The reduction in friction was more pronounced at higher speeds and loads, which aligns with the hypothesis that textures act as micro-reservoirs, enhancing lubrication under more demanding conditions. However, the introduction of grooves also led to a decrease in load-carrying capacity, particularly when deep grooves were used. This is because the grooves reduce the contact area and, consequently, the amount of load that can be supported by the hydrodynamic pressure. The study [44] found that shallow grooves with a higher number of grooves distributed evenly across the surface provided the best compromise between friction reduction and load-carrying capacity. The study [44] also highlighted the complex interaction between groove depth, the number of grooves, and operating conditions. For instance, while deeper grooves generally led to greater friction reduction, they also caused more significant drops in load-carrying capacity. Conversely, shallow grooves provided a more balanced performance, particularly at high speeds and loads.

the study [44] concludes that surface texturing, specifically the use of transverse grooves normal to the sliding direction, can substantially improve the frictional performance of journal bearings. The optimization of groove geometry is highly dependent on the specific operating conditions, including the load applied to the interface and the rotational speed of the bearing. For practical applications, the study [44] suggests that shallow grooves with sufficient numbers should be used to achieve the best balance between friction reduction and load-carrying capacity. The findings also emphasize the need for application-specific optimization, as the optimal texture geometry varies with operating conditions. According to Ali Usman and Ceol Woo Park [44] this work provides a valuable contribution to the field of tribology, offering insights into how surface texturing can be leveraged to enhance the performance of journal bearings in various industrial applications.

By combining advanced numerical modelling with systematic optimization, the study by Usman A and Park CW [44] provides a robust framework for designing surface textures that improve the efficiency and reliability of journal bearings. These findings are particularly relevant for industries where rotary machines are subject to varying loads and speeds, and where the reduction of friction and wear is critical to operational efficiency and component longevity.

6.2 Research N2

Wang L, Guo S, Wei Y, Yuan G, Geng H. [47] also present an interesting way of improving the tribological performance of journal bearings in their paper – “Optimization research on the lubrication characteristics for friction pairs surface of journal bearings with micro texture” [47]. The article delves into the intricate mechanisms and optimization strategies for improving the lubrication performance of journal bearings through the application of surface micro textures. The study aims to enhance the tribological properties of journal bearings by systematically investigating the influence of micro texture parameters on lubrication performance [47].

The study by Wang et al. [47] explores parameters such as texture shape, depth, density, and distribution in detail, using both theoretical models and experimental validation to identify the optimal micro texture configurations for journal bearings. The research focuses on understanding how different micro texture designs influence the lubrication characteristics under various operating conditions. The authors begin by establishing a theoretical framework for analysing the lubrication characteristics of journal bearings with micro textures. They employ the Reynolds equation, a fundamental equation in fluid dynamics that describes the pressure distribution in a thin lubricant film between two surfaces. The Reynolds equation is modified to account for the presence of micro textures on the bearing surface. The study considers a variety of micro texture shapes, including dimples, grooves, and ridges, and examines their impact on the pressure distribution and load-carrying capacity of the lubricant film [47]. The authors also explore the effect of texture density, which refers to the proportion of the bearing surface covered by micro textures, as well as the depth of the textures [47].

To validate their theoretical findings, Wang et al. [47] conducted a series of experiments using journal bearings with different micro texture designs. These experiments were performed under controlled conditions, with precise measurements of frictional forces, wear rates, and lubricant film thickness. The experimental results confirmed that micro textures can indeed enhance the lubrication performance of journal bearings. Specifically, the study found that certain texture configurations significantly increased the load-carrying capacity of the lubricant film while reducing friction and wear. The optimal texture parameters identified in the study include a moderate texture depth and a high density of evenly distributed dimples [47].

One of the key contributions of this research is the optimization of micro texture parameters to achieve the best possible lubrication performance. The authors used a combination of theoretical analysis and experimental data to develop a set of guidelines for designing micro textures on journal bearings. The study identified that the optimal texture depth is around 3-5 micrometres for most applications. This depth provides a good balance between enhancing hydrodynamic pressure and maintaining sufficient lubricant film thickness. Additionally, the authors Wang et al. [47] recommend a texture density of 15-25%, meaning that 15-25% of the bearing surface should be covered with micro textures. This density ensures that the textures are effective in improving lubrication without compromising the structural integrity of the bearing. Furthermore, the study suggests that the shape of the micro textures should be carefully chosen based on the specific operating conditions of the journal bearing. For instance, dimples are particularly effective in applications where the bearing operates under moderate loads and speeds, while grooves may be more suitable for high-speed applications where the lubricant flow needs to be guided in a specific direction [47].

The findings of this study have significant implications for the design and manufacturing of journal bearings. By incorporating optimized micro textures into the bearing surface, manufacturers can produce bearings with superior lubrication performance, leading to longer service life, reduced maintenance costs, and improved efficiency in mechanical systems [47]. The research also highlights the potential for applying surface texturing techniques to other types of bearings and friction pairs. For example, rolling element bearings, thrust bearings, and even seals could benefit from similar optimization strategies. The use of micro textures could also be extended to applications in aerospace, automotive, and industrial machinery, where high performance and reliability are critical [47]. The study by Wang et al. [47] represents a significant advancement in the field of tribology, particularly in the optimization of lubrication characteristics for journal bearings. The research demonstrates that surface micro textures can be effectively used to enhance the performance of journal bearings, provided that the texture parameters are carefully optimized. The combination of theoretical modelling and experimental validation provides a robust framework for designing micro textures that meet the specific needs of various applications [47].

In conclusion, the optimization of micro textures on journal bearings offers a promising approach to improving the efficiency and durability of rotating machinery. As surface texturing techniques continue to evolve, we can expect to see even greater improvements in the performance of journal bearings and other critical components in mechanical systems [47].

7 Development of the optimisation process of journal bearing

The development of such a computational model that describes the processes taking place in the journal bearing with sufficient accuracy and speed in many different operating conditions is the main idea and goal of this approach. The models presented above, the Reynolds equation, CFD and EHD models, are the main computational methods that are widely used in journal bearing optimization and other similar applications. However, as it was mentioned in their description, CFD and EHD, despite their advanced computational features, the time they need for a complete numerical calculation often requires hours and at the same time computers with powerful data. Considering these factors, these models do not allow to be selected for such jobs where repetitive tasks will be performed during hundreds of thousands of operating conditions. A suitable reporting model should more or less meet these conditions to characterize the process with sufficient physical depth and reasonable speed to handle thousands of individual computations on available computers.

For my application I chose to use the model presented in [30]. In this study, Novotný, Jonák, and Vacula [30] explore the optimization of thrust bearings in turbomachinery. They consider various operating conditions and employ evolutionary techniques to enhance the performance of these critical components. The research contributes valuable insights to the field of mechanical engineering. This approach successfully meets the requirements presented above. However, since the model presented in [30] is dedicated to thrust bearing, it needs to be adapted for journal bearing application.

7.1 Modelling of journal bearing lubricant flow

7.1.1 Defining the bearing geometry

Governing equation of this model is three-dimensional Reynold's equation (15) which was presented previously from the source [38]:

$$(15)\quad \frac{\partial}{\partial x}\left(\frac{h^3}{\eta}\frac{\partial p}{\partial x}\right)+\frac{\partial}{\partial y}\left(\frac{h^3}{\eta}\frac{\partial p}{\partial y}\right)=6\left(U\frac{\partial h}{\partial x}+V\frac{\partial h}{\partial y}\right)+12(w_h-w_0).$$

Farther simplifications and changes will be made on this equation before apply it in calculations but first, bearing geometry must be defined. Farther geometric analisis for expressing lubrican film thickness function will be baced on the source [40].

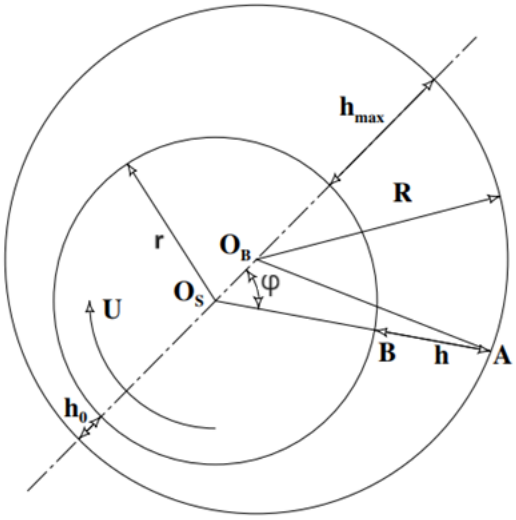

Figure 16. Journal bearing geometry [40].

Where R represents bush radius, r is shaft radius, O_b and O_s are centres of the bush and the shaft respectively [40]. For geometric analysis, we need to observe the triangle O_bO_sA presented on figure (17) :

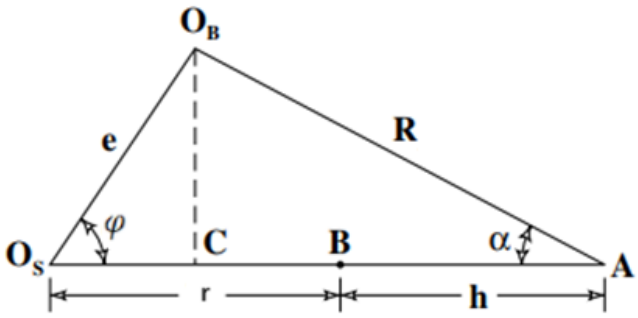

Figure 17. Details of geometry for the evaluation of film shape in journal bearings [40].

Here e represents a distance between centres of the shaft and the housing and is called eccentricity. h is the film thickness and φ is the angle by which the journal is rotated with respect to housing [40]. From this triangle based on the source [40] it can be written that:

$O_sA = O_sC + CA = O_sB + BA$ or $O_sA = ecos\varphi + Rcos\alpha = r + h.$

from there it can be said that: (19) $h = ecos\varphi + Rcos\alpha - r.$

from the basic trigonometry we know that $\frac{e}{sin\alpha} = \frac{R}{sin\varphi}$ and $cos\alpha = \sqrt{1 - sin^2\alpha}.$

combining this two, rules we get: $cos\alpha = \sqrt{1 - \left(\frac{e}{R}\right)^2 sin^2\varphi}.$

Since $\frac{e}{R} \ll 1$ then: $cos\alpha \approx 1$ and by substituting this back to (19) we get:

$h = ecos\varphi + R - r$. Denoting that $R - r = c$ and $\frac{e}{c} = \varepsilon$ it yields:

$$(20)\ h = c(1 + \varepsilon cos\varphi)$$

Where c represents radial clearance and ε is eccentricity ratio.

7.1.2 Effective angular velocity

In a continues event the shaft (pin) changes position and the size of the minimum gap. Graphically it can be shown on the figures 18 and 19 [33]. Farther analyses and derivation of effective angular velocity will be based on the source [33].

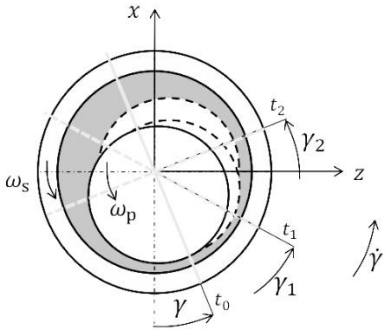

Figure 18. Position change of minimum gap [33].

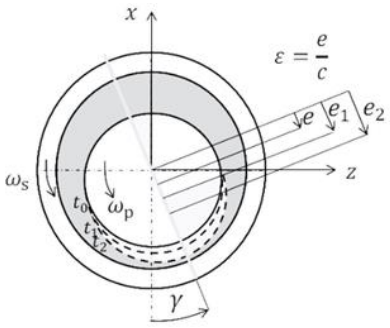

Figure 19. Changing of minimum gap thickness [33].

Where ω_p and ω_b are shaft (pivot) and bush (stationary pan) angular speeds respectively. However, in this case bush is fixed, which means that $\omega_b = 0$. The angular speed of minimum gap position changing is γ', γ is minimum gap angle and ε is relative eccentricity. Change of the position of the minimum gap (pivot spinning) can be expressed this way: $\gamma' = \frac{d\gamma}{dt}$ and with the same manner rate of change of the relative eccentricity will be $\varepsilon' = \frac{d\varepsilon}{dt}$. However, the angular changing rate of the minimum gap (γ') applies only to a continuous process. Therefore, since the angular speed of housing is also zero ($\omega_b = 0$) effective angular speed, originally expressed in this way:

$\omega_e = \omega_p + \omega_b - 2\gamma'$, for the steady state operating conditions will be equal to shaft angular speed: $\omega_e = \omega_p$.

Substituting (20) in the equation (15) and rewriting it in cylindrical coordinates considering with effective angular speed (ω_e), $x = rcos\varphi$, $z = rsin\varphi$, velocity along the shaft equals zero ($V = 0$), also using dimensionless quantities ε and $\frac{r}{c}$, for steady state operating conditions we will get:

$$(21)\ \frac{\partial}{\partial\varphi}\left((1\ +\ \varepsilon cos\varphi)^3\ \frac{\partial p}{\partial\varphi}\right)+r^2\frac{\partial}{\partial y}\left((1\ +\ \varepsilon cos\varphi)^3\ \frac{\partial p}{\partial y}\right)=-6\eta\left(\frac{r}{c}\right)^2(\omega_e\varepsilon sin\varphi).$$

7.1.3 Pressure distribution

In this specific case bearing diameter "d" and bearing length "b" are in such ranges that ratio $\frac{d}{b}<\frac{1}{3}$. According to the source [40] it allows to use short bearing theory, according to which pressure gradient along the x axis can be neglected because of its greatly less value, in another words $\partial p/\partial\varphi=0$. Therefore, by applying short bearing approximation in (21) first term of the left side of the equation becomes zero and it yields:

$$(22)\ \frac{\partial}{\partial y}\left((1\ +\ \varepsilon cos\varphi)^3\ \frac{\partial p}{\partial y}\right)=-\frac{6\eta}{c^2}(\omega_e\varepsilon sin\varphi-2\varepsilon' cos\varphi).$$

From now, for defining pressure function farther derivations based on the source [38] will be made in cartesian coordinates and later the answer will be presented back to cylindrical coordinates.

Since $h\neq f(y)$, farther simplification gives:

$$(23)\ \frac{d^2p}{dy^2}=\frac{6U\eta}{h^3}\ \frac{dh}{dx}.$$

By integrating equation (23) twice we get:

$$(24)\ p=\frac{6U\eta}{h^3}\ \frac{dh}{dx}y+C_1 \qquad \text{and} \qquad (25)\ p=\frac{6U\eta}{h^3}\ \frac{dh}{dx}\frac{y^2}{2}+C_1y+C_2.$$

To define integration constants C_1 and C_2 boundary conditions must be defined. Boundary conditions are:

$$p=p_{in} \qquad \text{at} \qquad y=\pm\frac{b}{2} \qquad \text{and} \qquad \frac{\partial p}{\partial y}=0 \qquad \text{at} \qquad y=0.$$

Where pin is inlet pressure of the oil by which the bearing is supplied. By Substituting boundary conditions in (24) and (25) constants C_1 and C_2 will be defined:

$$C_1=0 \quad \text{and} \quad C_2=p_{in}+\frac{3U\eta}{h^3}\ \frac{dh}{dx}\frac{b^2}{4}.$$

substituting C_1 and C_2 back to (25) the pressure distribution will have this face:

$$(26)\ p=p_{in}+\frac{3U\eta}{h^3}\ \frac{dh}{dx}\left(y^2-\frac{b^2}{4}\right).$$

Now, presenting x as angular displacement times radius gives: $x=R\varphi$ and differentiation will give: $dx=rd\varphi$ [40]. After substituting back to (26) we get:

$$(27)\ \ p=p_{in}+\frac{3U\eta}{h^3r}\ \frac{dh}{d\varphi}\left(y^2-\frac{b^2}{4}\right).$$

By differentiating equation (20), from the source [40] it can be written that: $\frac{dh}{d\varphi}=-c\varepsilon sin\varphi$. And finally, also based on [40], by substituting h expressed from (20) and

$\frac{dh}{d\varphi}$ in the (27) the pressure distribution function in the hydrodynamic lubricating film in terms of bearing geometry, lubricant viscosity and speed under short bearing theory is obtained:

$$(28)\quad p = p_{in} + \frac{3U\eta\varepsilon sin\varphi}{rc^2(1+\varepsilon cos\varphi)^3}\left(\frac{b^2}{4} - y^2\right).$$

Equation (28) in cylindrical coordinates under steady state operating condition will be:

$$(28.1)\quad p = p_{in} + \frac{3\eta}{c^2(1+\varepsilon cos\varphi)^3}\omega_e\varepsilon sin\varphi\left(\frac{b^2}{4} - y^2\right).$$

The formation of hydrodynamic pressure is assumed only in angular range $0 < \varphi < \pi$. In the remaining range $\pi < \varphi < 2\pi$ the pressure is assumed according to bearing's cavitation properties, which in this case would equal to p_{in}. Graphical representation of pressure distribution is shown in figure 20.

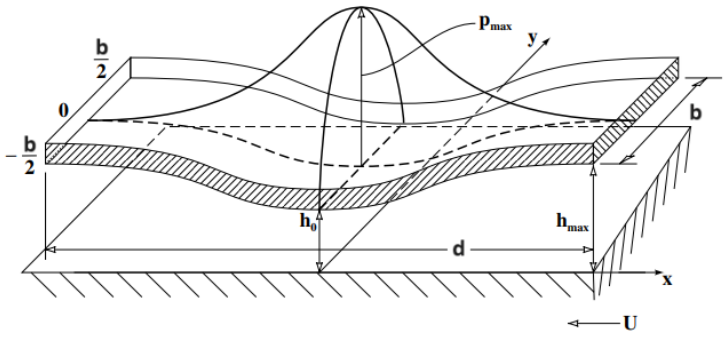

Figure 20. Pressure distribution in short bearing approximation [38].

7.1.4 Load capacity

Load capacity is obtained by Integration of the hydrodynamic pressure distribution over the bearing surface. Here will be used Half-Sommerfeld condition, which means that negative pressure in the second half of the bearing (the area from π to 2π) is neglected [40]. According to the source [40] considering that area of small element is "$rd\varphi dy$", load acting on it will be: $prd\varphi dy$. However, as usual, load is calculated from two components: F_r and F_t. One acts along the line which connects the centres of the housing and the journal and the second acts perpendicular to the first one. Therefore, these two components based on the source [40] can be expressed this way:

$$(29)\ F_r = \int_0^{\pi}\int_{-\frac{b}{2}}^{\frac{b}{2}} prcos\varphi d\varphi dy \quad \text{and} \quad (30)\ F_t = \int_0^{\pi}\int_{-\frac{b}{2}}^{\frac{b}{2}} prsin\varphi d\varphi dy.$$

Loads and pressure field acting in the bearing is shown in figure 21:

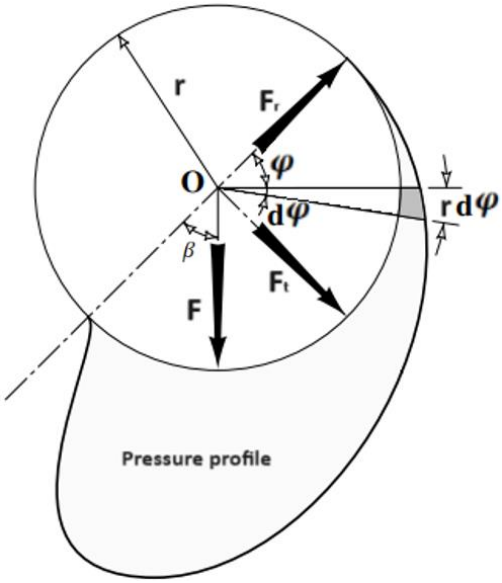

Figure 21. Load components and pressure field in a journal bearing [40].

By substituting expression of p from equation (28), farther integrations based on [40] give:

$$(31)\ F_r = -\frac{U\eta d^3\varepsilon^2}{c^2(1-\varepsilon^2)^2} \qquad \text{and} \qquad (32)\ F_t = \frac{U\eta\varepsilon\pi b^3}{4c^2(1-\varepsilon^2)^{\frac{3}{2}}} - p_{in}rb.$$

In the equation (32) the second term can be neglected due to its small value [40], thus it gets:

$$(33)\ F_t = \frac{U\eta\varepsilon\pi b^3}{4c^2(1-\varepsilon^2)^{\frac{3}{2}}}.$$

Finaly, total load F can be obtained by geometric summation of F_r and F_t:

$$(34)\quad F = \frac{U\eta\varepsilon b^3}{c^2(1-\varepsilon^2)^2}\frac{\pi}{4}\sqrt{\left(\frac{16}{\pi}-1\right)\varepsilon^2+1}\,.$$

In the cylindrical coordinates it will be:

$$(35)\quad F = \frac{\eta\omega_e b^3}{2r}\left(\frac{r}{c}\right)^2\left(\frac{\pi\varepsilon}{2(1-\varepsilon^2)^2}\sqrt{(1-\varepsilon^2)+\left(\frac{4\varepsilon}{\pi}\right)^2}\right).$$

7.1.5 Friction force

For calculating the friction force source [40] is used and based on it, there can be used the same approach as it was for load capacity, but here it can be obtained by integrating the shear stress over the shaft surface:

$$(36) \quad F_f = \int_0^b \int_0^d \tau dx dy \,.$$

By substituting τ from expression (4) $\tau = \eta \frac{du}{dz}$ [39] it gives:

$$(37) \quad F_f = \int_0^b \int_0^d \eta \frac{du}{dz} dx dy \,.$$

In this specific case semi-floating ring bearing is used, which means that housing is fixed and only shaft rotates. Thus, $U_1 = u$ and $U_2 = 0$. Substitution of expression of "u" from (9) [38] considering that $U_2 = 0$ and using short bearing approximation, that is $\frac{\partial p}{\partial x} \approx 0$ since $\frac{\partial p}{\partial x} \ll \frac{\partial p}{\partial y}$, equation (37) becomes:

$$(37) \; F_f = \int_0^d \frac{u\eta b}{h} dx \,.$$

Substituting "h" from (20) and considering that $dx = Rd\theta$, we get:

$$(38) \quad F_f = \frac{u\eta br}{c} \int_0^\pi \frac{d\varphi}{(1+\varepsilon cos\varphi)} \quad .$$

Finaly, considering that $u = \omega_e r$, integration gives:

$$(39) \quad F_f = \frac{2\pi u\eta br}{c} \frac{1}{(1+\varepsilon^2)^{0.5}} \,.$$

7.1.6 Friction coefficient

Since expressions of load capacity and friction force are obtained, based on the source [40] Friction coefficient can be calculated in this way:

$$(40) \quad \mu = \frac{F_f}{F} \,.$$

Substituting F_f and F from (39) and (35) gives an expression of friction coefficient with Half-Sommerfeld condition:

$$(41) \quad \mu = \frac{8rc}{b^2 \varepsilon} \frac{\left(1-\varepsilon^2\right)^{1.5}}{(0.621\varepsilon^2+1)^{0.5}} \,.$$

7.1.7 Lubricant flow rate

According to the source [40] to calculate flow rate equation (13) there can be used with additional simplification, that, since for short bearing applications pressure gradient along the x direction is neglected ($p/\partial x \approx 0$), therefore:

$$(42) \quad q_x = \frac{uh}{2} \,.$$

Substituting h from the (20) and integrating flow equation over the bearing width gives lubricant flow in the bearing:

$$(43) \quad Q_x = \frac{ub}{2}c(1 + \varepsilon cos\varphi).$$

In journal bearings it is important to consider side leakage or, in another words, side flow to provide sufficient lubricant supply and therefore prevent lubricant starvation. Lubricant supply rate can be calculated by the difference between lubricant inflow and outflow. Graphical representation is given in figure 22.

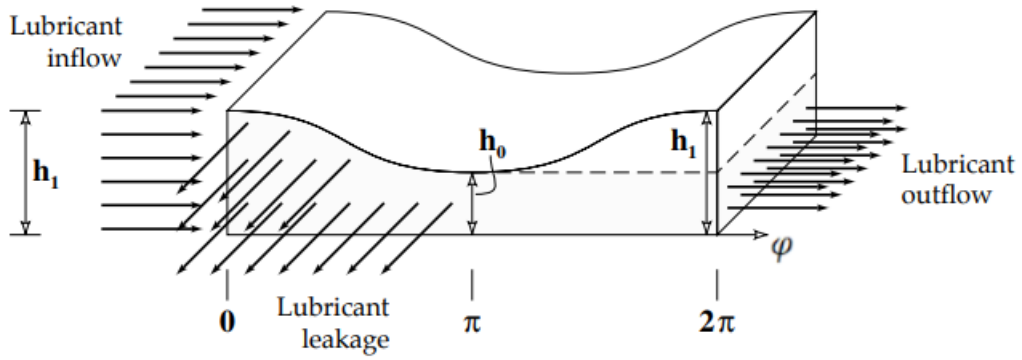

Figure 22. lubricant flow in journal bearing [40].

Where h_1 is the maximum film thickness and h_0 is the minimal film thickness. As it can be seen from the figure (22) when lubricant flows inside the bearing $\varphi = 0$ and film thickness $h = h_1$ and for the outflow $\varphi = \pi$ and $h = h_0$. To calculate the difference between inflow and outflow of the lubricant, these boundary conditions need to be applied in the equation (43), then it gives:

$$(44) \quad Q_1 = \frac{ub}{2}c(1 + \varepsilon) \qquad \text{and} \qquad (45) \quad Q_0 = \frac{ub}{2}c(1 - \varepsilon).$$

Considering that $u = \omega_e r$ it yields:

$$(46) \quad Q_1 = \frac{\omega_e rb}{2}c(1 + \varepsilon) \qquad \text{and} \qquad (47) \quad Q_0 = \frac{\omega_e rb}{2}c(1 - \varepsilon).$$

Lubricant leakage would be: $Q = Q_1 - Q_0$.

Substituting Q_1 and Q_0, gives:

$$(48) \quad Q = \omega_e rcb\varepsilon .$$

To calculate side mass flow, it is necessary to add a lubricant density ρ in the equation. Lubricant mass flow in journal bearing can be expressed this way:

$$(49) \quad \dot{m} = \rho\omega_e rcb\varepsilon .$$

7.1.8 Lubricant supply

Side mass flow expressed in (49) is actual amount of lubricant that journal bearing requires from supply system. To provide lubricant supply in the bearing hole or groove must be drilled in it. In this case, hole will be used with the same manner as it is shown in figure 23 [40]. A hole is drilled into the bush of nearly every bearing at a location that is distant from the point directly beneath the load [40].

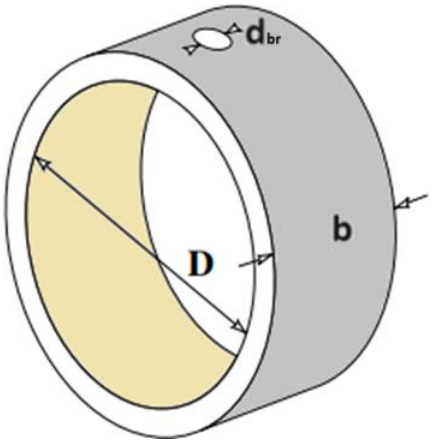

Figure 23. lubricant supply hole in journal bearing [40].

Based on the source [40] total flow Q from a groove or supply hole into a bearing consists of two parts: the forced flow Q_{pr} from the externally pressurised lubricant and the net Couette flow Q_c, which is caused by the difference in film thickness between the groove/hole's upstream and downstream sides. Formula is: $Q = Q_c + Q_{pr}$ [40]. However, for small holes and grooves $Q_c = 0$, therefore in this specific case we get:

$$(50) \quad Q = Q_{pr} \, .$$

Pressurized oil flow for small supply holes ($d_h < b/2$) can be obtained from this formula:

$$(51) \quad Q_{pr} = 0.675 \frac{p_{in} {h_{br}}^3}{\eta} \left(\frac{d_{br}}{b} + 0.4 \right)^{1.75} \qquad [40]$$

Where p_{in} is inlet pressure, h_{br} is film thickness at the position of hole and d_{br} is diameter of the supply hole. For sufficient selection of the supply hole position in the bearing value of h_{br} can be calculated from the equation (51) for specific optimised bearing geometry [40].

7.1.9 Outlet temperature

Lubricant temperature in journal bearings rises due to shear stress. The thermal energy generated by shear stress per second for this specific case can be calculated from the basic expression of friction power for rotating systems [31]. Derivation is from the source [31].

$$(52) \quad E = M_f \omega_e$$

Where M_f represents friction torque and can be obtain from this:

$$M_f = F_f r \quad (53)$$

Since the same energy is dissipated by the lubricant flow, from the general thermodynamics for this specific case it can be written:

$$E = M_f \omega_e = \dot{m} c_p (T_{out} + T_{in}) \quad (54)$$

Rearranging the last equation with respect to T_{out} gives:

$$T_{out} = T_{in} + \frac{M_f \omega_e}{\dot{m} c_p} \quad (55)$$

7.2 Operating conditions of turbocharger used for the journal bearing optimisation

For optimisation of bearing performance steady state operating conditions are considered. Optimised bearing geometry that is to be obtained under five different working conditions of turbocharger is defined below in the table 2.

Table 2. operating conditions [33].

	Preferred design operational Conditions ↙ ↓ ↘			**Out-off design operational conditions** ↙ ↘	
Operating conditions	**Low speed**	**Mid. speed**	**High speed**	**Very low speed 1**	**Very low speed 2**
Rotor speed, n [rpm]	20000	30000	40000	5000	2000
Load capacity, F [N]	100	100	150	100	100
Inlet oil pressure p_{in} [bar]	1.7	1.7	1.7	1.7	1.7
Oil inlet temperature, T_{in} [°C]	80	80	80	80	80
Weight factor, W [-]	0.3	0.3	0.3	0.05	0.05

7.3 Adaptation of Genetic Algorithms

For solving this optimisation problem there will be used genetic algorithms (GA). The GA is an approach known as heuristics that applies the concepts of evolutionary biology to solve problems for which there isn't a workable, precise algorithm [32]. The terms

"individual," "generation," "gene," "objective function," and "fitness function" are used to describe problematics. The ideal journal bearing parameters are found by using the journal bearing parameters listed in the preceding paragraphs. A collection of variables (genes) represents each solution (an individual), and integral features (the objective function) are used to evaluate each solution. The objective function is used to compute each person's fitness function in order to produce a new generation. Thus, depending on the genes, the algorithm looks for the global minimum of the objective function. The fitness function in this instance expresses the quality of the thrust bearing design as represented by the individual and is expressed as a negative value of the objective function. The genetic operators choose and modify individuals systematically through selection, crossover, and mutation. A new generation is produced following the use of these genetic operators. A generation model of GA limited by elitism and gene limit values is part of the suggested approach. With each iteration of this model, a new generation of individuals is produced, and a fixed percentage of the best individuals (also known as elite individuals) from the previous generation are kept [32].

To optimise the journal bearing, considering the same approach as it is presented in the source [32], the integral characteristics of its current serial design, whose working circumstances are identical as shown in Table 2, are compared. Initial bearing parameters will be denoted with index "$init$". The geometry of the initial bearing is $r_{init} = 15\text{mm}$, $c_{init} = 0.025\text{ mm}$ and $b_{init} = 15\text{mm}$.

the primary objective of the optimisation is to minimise friction torque in the bearing while considering limits of minimal film thickness (h_m) and maximum pressure (p_{max}). The objective function f_{obj} that must be minimised is presented in this form:

$$(56)\ f_{obj} = \frac{\sum_{i=1}^{N_{max}} f_{FTR,i}\, S_{p,i}\, S_{h,i}\, W_i}{\sum_{i=1}^{N_{max}} w_i}.$$

Where, N_{max} is maximum number of operating conditions used for the optimisation. In this case $N_{max} = 5$. A ratio between new friction torque obtained during optimisation process and initial friction torque under each specific operating condition is presented with f_{FTR} . according to its explanation this term can be expressed in following way:

$$(57)\ f_{FTR} = \frac{M_f}{M_{f,init}}.$$

S_p and S_h are the pressure and the film thickness factors respectively. they rise the value of the objective function when the limiting pressure or/and limited film thickness is exceeded [32]. they are expressed in this form:

$$(58)\ S_p = max\left(\left(\frac{p_{max}}{p_{lim}}\right)^{\lambda}, 1\right) \quad \text{and} \quad (59)\ S_h = max\left(\left(\frac{h_{lim}}{h_0}\right)^{\lambda}, 1\right).$$

An undesirable value for the lubrication gap thickness or/and hydrodynamic maximum pressure raises the objective function value and lowers the individual's fitness function. this is determined by the power exponent λ, which in both cases is chosen as the value of 3 [32].

W represents a weight factor for each operating conditions. Presenting weight factor in calculation is a way of solution of problem when importance of given operating conditions are unequal. Weight factor values for each condition are shown in table 2.

Variables are presented in specific ranges where from a specific combination of values is taken for each step and new individuals are created. Number of steps, or in another words division of ranges depends on the user. In this case each variable range is divided in 100 steps. Initial data and limits of parameters are shown in table 3.

Table 3. initial data and limits of parameters [33].

Parameter	**Parameter value**
Shaft diameter range	$d = 29 \div 31\text{mm}$
Bearing width range	$b = 10 \div 20\ \text{mm}$
Radial clearance range	$c = 0.050 \div 0.060\ \text{mm}$
Oil density	$\rho = 850\ \text{kg} \cdot \text{m}^{-3}$
Oil viscosity	$\eta = 0.01\ \text{Pa} \cdot \text{s}$
Specific heat capacity	$c_p = 2320\ \text{Jkg}^{-1}\text{K}^{-1}$
Input pressure	$p_{in} = 1.7\ \text{bar}$
Output pressure	$p_{out} = 1\ \text{bar}$
Diameter of oil input bores 4 x 90°	$d_{br} = 2\ \text{mm}$
Limit of layer thickness	$h_{lim} = 0.01\ \text{mm}$
Limit of pressure	$p_{lim} = 50\ \text{MPa}$

In the optimisation process new generations are created until it meets a condition after which the process stops. Several stopping criteria are used in this optimisation. These criteria are designed to prevent the GA from running indefinitely while ensuring that it converges towards an optimal or near-optimal solution [32]. These criteria are: Maximum generations, Function tolerance, Maximum stall generations and Population size [32]. First criterion is set to run for a maximum 100 generations which ensures that the algorithm does not continue to iterate indefinitely, providing a balance between computational efficiency and solution quality. If the algorithm reaches 100 generations without meeting other stopping criteria, it terminates [32]. As for the function tolerance, its value of 10^6 was used to monitor the

improvement in the best fitness value across generations. The algorithm stops when the average change in the fitness value falls below this threshold, indicating that further improvements are minimal, and the solution is likely close to optimal [32]. To avoid unnecessary computations when no significant progress is being made, the criterion of "maximum stall generations" is set to stop optimisation process if there was no improvement in the best fitness value for 50 consecutive generations. This criterion helps in terminating the algorithm early if it gets stuck in a local optimum or if the population has converged [32]. The population size was set to 50, meaning that each generation consisted of 50 individuals (solutions). While not a direct stopping criterion, the population size influences the computational load and the diversity of solutions. A larger population can explore more of the solution space but requires more computational resources [32].

8 Results and discussion

This optimisation method built on the GA is developed to be capable to discover the optimal journal bearing design, considering numerous design factors under many operating situations. Optimisation process was numerically solved in MATLAB online, for which I used my student license trough VUT portal.

Optimisation process took 15-20 seconds. Such a small time for solving the problem is caused due toe few numbers of variables (3 variables) and operating conditions (only 5 operating conditions). However, in engineering practice there are much longer computation periods when solving such problems for higher number of variables and operating conditions. For example, in case of the study of Novotný, Jonák, and Vacula [30] where GA was also used for complete computation it took approximately 24 hours. Due to such short calculation time, in my case it was possible to use the brute force method instead of GA. Of course, this method would take a relatively long time, since the algorithm does not contain stopping criteria, but calculations were also performed using this method for the exact same problem, which took only a few seconds more time than in the case of GA. However, it should be noted again that such a small difference in time is explained by the simplicity of this particular case report, and that in other more complex cases the difference will be much higher than a few seconds.

After meeting the stopping criteria, the optimal geometry of the journal bearing was obtained along with other search parameters. Table (4) shows the optimal geometric dimensions. Figures (24-30) show comparisons of the theoretically obtained operating parameters of the optimized journal bearing and the initial serial journal bearing against the turbocharger shaft speed.

Table 4. Optimal values of journal bearing geometry.

Parameter	Parameter value
Bearing diameter	$d = 29.00$ mm
Bearing width	$b = 10.00$ mm
Radial clearance (Diametral)	$c = 0.0599$ mm

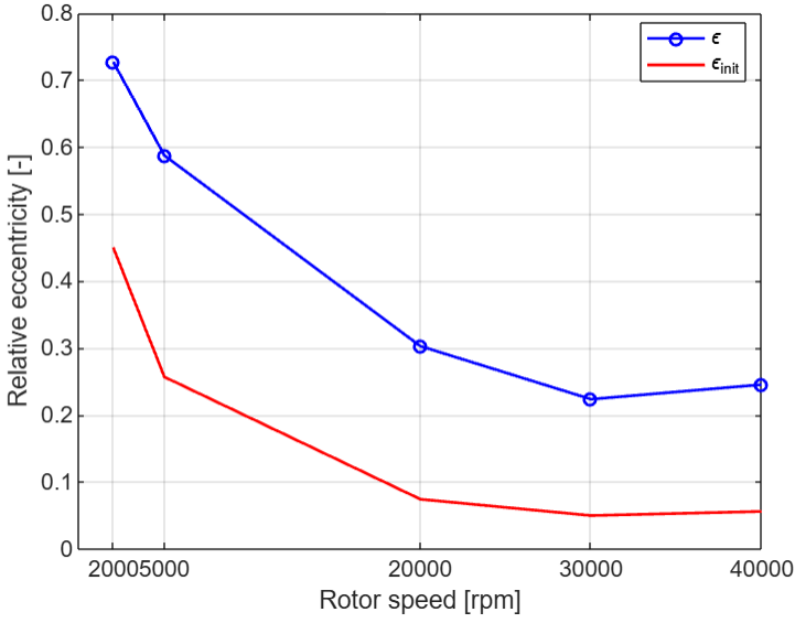

Figure 24. Relation between relative eccentricity and turbocharger rotor speed.

On the figure 24 blue line represents new value of eccentricity ratio ε and red line shows change of initial bearing relative eccentricity "ε_{init}" with respect to rotor speed. As it is shown in the new bearing values of "ε" lies over its initial values, which itself let us predict that minimal film thicknesses may be lower in the new bearing, but it also depends on bearing geometry and more accurate visualisation of film thickness I shown in the figure 25.

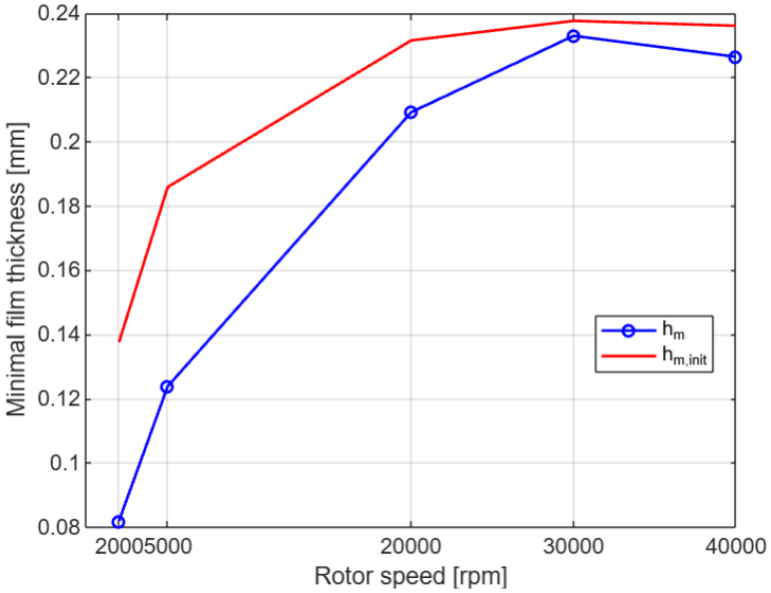

Figure 25. Relation between minimal film thickness and turbocharger rotor speed.

There can clearly be seen the change of new and initial bearing minimum film thicknesses with respect to rotor speed. It can be claimed that due to optimisation process film thickness for the new bearing is taken lower than it was in the previous case, since as it is known from Stribeck graph (figure 10. [24]) that under stable operation of bearing hydrodynamic friction coefficient and therefore friction force reduces as the film thickness decreases. Figure 26 shows mass flow rate difference with respect to rotor speed for the new and the initial bearing cases.

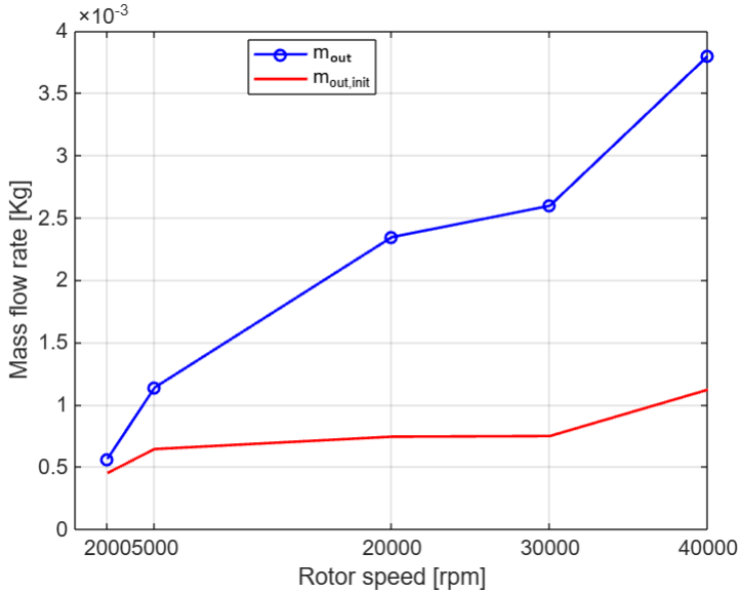

Figure 26. Relation between lubricant mass flow rate and turbocharger rotor speed.

For the new bearing higher oil consumption is obtained and it also can be seen that difference between earlier and new bearing oil flow rates increases as the rotor speed rises. At the first analysing steps higher mass flow rate intuitively should reduce temperature rise of

the lubricant and as it can be seen on the figure 27 and figure 28 thermal conditions are highly improved for the new bearing.

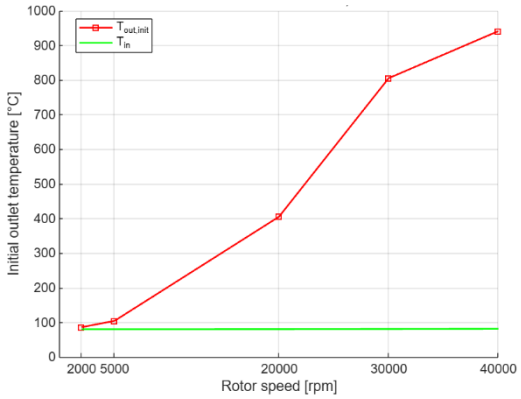

Figure 27. Relation between lubricant outlet temperature and turbocharger rotor speed in the initial bearing.

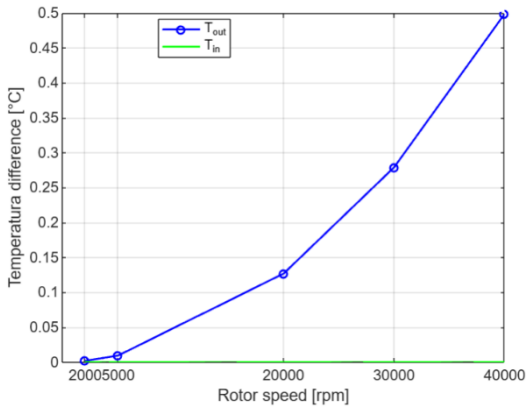

Figure 28. Relation between lubricant outlet temperature rise and turbocharger rotor speed in the new bearing.

As for the friction force and friction torque noticeable theoretical improvement are achieved. From 1.48 to 1.87 times lower friction forces and from 1.53 to 1.93 times lower friction torques are obtained comparing to their initial values. Graphically it is shown in figures 29-30.

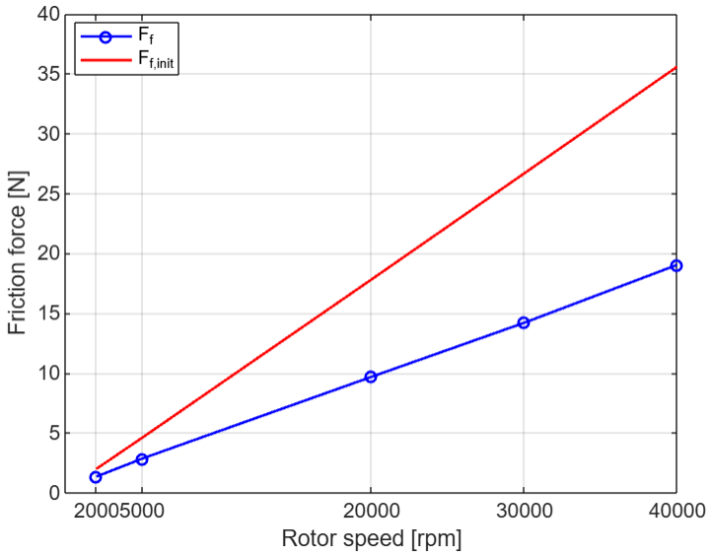

Figure 29. Relation between hydrodynamic friction force in the journal bearing and turbocharger rotor speed.

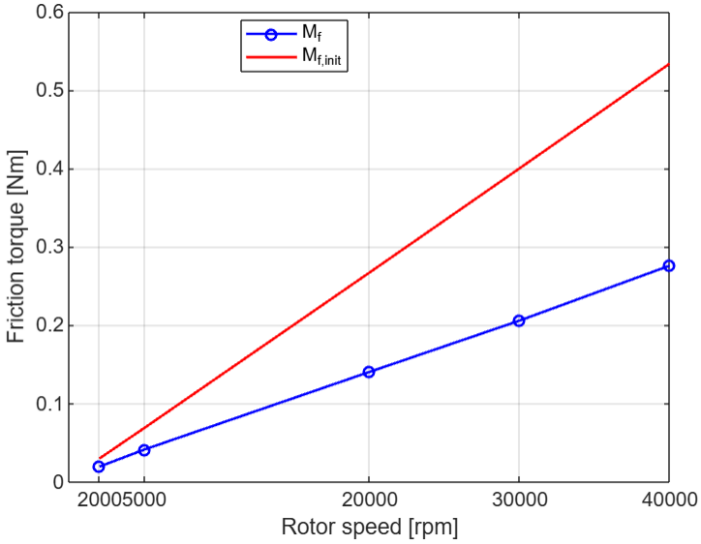

Figure 30. Relation between hydrodynamic friction torque in the journal bearing and turbocharger rotor speed.

All results presented above are theoretical expectations and require experimental evaluation for complete recognition.

9 Conclusion

Presented approach is characterised with sufficient computational model of lubrication in journal bearing and solves the optimisation problem by using genetic algorithm (GA). Together with the effective bearing model, the method demonstrates great numerical stability, good convergence and meets the requirements of reasonable calculation time and physical depth. The idea that the optimisation strategy looks for the objective function's global maximum (for negative objective function) from a predetermined ranges of parameter values is a key component. In engineering practice, these intervals denote certain actual restrictions, such as those that are structural or technical in character.

This approach makes it possible to obtain optimal design of journal bearing to achieve more effective operating results under determined several operating conditions. Some condition, as they can be seen above, are given higher weight factor, in another words, higher importance which have significant influence on designing of new bearing geometry. On the other hand, off-design operating conditions, nevertheless their significantly lower weight factor they still have a positive influence and let the bearing more or less maintain stability under emergency situations. Basically, when it comes to developing a computational model, the choice is made between its physical depth and speed of solution. In this particular case, as it turned out, considering the time factor was not a priority due to the small number of variables and operating conditions, although this particular optimization method can be freely used in many other engineering applications due to its robustness of the genetic algorithm and sufficient physical depth.

Despite everything, this optimization method also has some disadvantages. Analytical description of journal bearing is based on the theory of short bearing, and therefore due to this limitation, when it specifically comes to optimising a journal bearing, application of this method to other types of bearings requires multi-step adaptation. Also, doe to the fact that GA inherently has certain qualities and incorporates them into the optimization process, it has some drawbacks of its own. In some cases, settings may prevent GA-based optimization from finding the global optimal solution. Nevertheless, the size of the starting population has a significant impact on the likelihood of discovering the global maximum. A larger population increases the likelihood of finding a global maximum, but the computing burden increases as well.

Finally, it can be said that the presented optimization method is reasonably flexible for many other engineering applications and that its effectiveness at the expense of fast calculation and deep physical analysis still takes a noteworthy role despite some of its limitations.

References

[1] Alsaeed AA. A study of methods for improving the dynamic stability of high-speed turbochargers (Doctoral dissertation, Virginia Tech). p. 1-11.

[2] BECZE ES. Research on the construction and operation of turbochargers in internal combustion engines (Doctoral dissertation, Technical University of Cluj Napoca).

[3] Blair GP, Goulburn JR. The pressure-time history in the exhaust system of a high-speed reciprocating internal combustion engine. sAe Transactions. 1968 Jan 1:1725-32.

[4] Bontempo R, Cardone M, Manna M, Vorraro G. Steady and unsteady experimental analysis of a turbocharger for automotive applications. Energy Convers Manag. 2015; 99:72–80.

[5] Brodbeck P, Guse E. Experimental Investigation of Twin Scroll Turbocharger Performance Under Pulsating Conditions. In: Proceedings of the ASME Turbo Expo 2022: Turbomachinery Technical Conference and Exposition. Rotterdam, Netherlands; June 13–17, 2022. Paper V007T18A004. ASME.

[6] Chatzisavvas I, Boyaci A, Koutsovasilis P, Schweizer B. Influence of the Oil Temperature of Thrust Bearings on the Vibratory Behavior of Small Turbochargers. 2015 Sep 7. p. 4.

[7] Chen L, Sun Y, Xu Z. Multigrid methods for EHD lubrication problems. Comput Math Appl. 2019;78(6):1849-1864.

[8] Chiong MS, Abas MA, Tan FX, Rajoo S, Martinez-Botas R, Fujita Y, Yokoyama T, Ibaraki S, Ebisu M. Steady-state, transient and WLTC. drive-cycle experimental performance

comparison between single-scroll and twin-scroll turbocharger turbine. SAE Technical Paper; 2019 Apr 2.

[9] Chiong MS, Rajoo S, Martinez-Botas RF, Costall AW. Engine turbocharger performance prediction: One-dimensional modeling of a twin entry turbine. Energy Conversion and Management. 2012; 57:68-78. ISSN 0196-8904.

[10] Deligant M, Podevin P, Descombes G. Experimental identification of turbocharger mechanical friction losses. Energy. 2012 Mar 1;39(1):388-94.

[11] Ebert FJ. Fundamentals of design and technology of rolling element bearings. Chinese Journal of Aeronautics. 2010 Feb 1;23(1):123-36.

[12] Feneley AJ, Pesiridis A, Andwari AM. Variable geometry turbocharger technologies for exhaust energy recovery and boosting-A Review. Renewable and sustainable energy reviews. 2017 May 1; 71:959-75.

[13] Flärdh O, Mårtensson J. Exhaust pressure modeling and control on an SI engine with VGT. Control Engineering Practice. 2014 Apr 1; 25:26-35.

[14] Gianluca Pasini, Giovanni Lutzemberger, Stefano Frigo, Silvia Marelli, Massimo Ceraolo, Roberto Gentili, and Massimo Capobianco conducted a study titled “Numerical Evaluation of an Electric Turbo Compound for SI Engines” published in the journal Applied Energy (Volume 162, 2016, Pages 527-540).

[15] Gupta K, Verma A, Singh P. Advances in elastohydrodynamic lubrication: a review. Tribol Int. 2022; 168:107460.

[16] Hamrock BJ, Anderson WJ. Rolling-element bearings. 1983 Jun 1.

[17] Hirani H, Sunil J. Computational Fluid Dynamics and Fluid-Structure Interaction Analysis of Journal Bearings. Proc Inst Mech Eng J J Eng Tribol. 2007;221(3):283-93.

[18] Hirani H. Basic models of lubrication. In: Fundamentals of Engineering Tribology with Applications. Cambridge University Press; 2016 Mar 11. p. 17.

[19] JH Lee, HY Kang, YW Kim, et al. Analysis of the life cycle environmental impact reductions of remanufactured turbochargers. Jnl Remanufactur. 2023; 13:187–206.

[20] Kumar M, Whittaker AS, Constantinou MC. Characterizing friction in sliding isolation bearings. Earthquake Engineering & Structural Dynamics. 2015 Jul 25;44(9):1409-25.

[21] Li CJ, McKee K. Diagnostics: Bearing (roller & Journal) vibrations and diagnostics. Encyclopedia of Vibration. 2001 Aug.

[22] Li X, Zhu H, Lu Y. Numerical Analysis of the Lubrication Performance of Journal Bearings with Oil Supply and Starved Lubrication. Tribol Int. 2008;41(3):222-32.

[23] Luo X, Fang T, Li J. Implementation of EHD lubrication models in turbocharger journal bearings. J Mech Eng. 2020;66(12):625-634.

[24] Mang T, Bobzin K, Bartels T. Industrial tribology: Tribosystems, friction, wear and surface engineering, lubrication. John Wiley & Sons; 2011 Jan 19.

[25] Moody JF. Variable Geometry Turbocharging with Electronic Control. SAE Trans. 1986; 95:552-62.

[26] Nguyen-Schäfer, H. (2012). Bearing Dynamics of Turbochargers. In: Rotordynamics of Automotive Turbochargers (pp. 127-189). Springer, Berlin, Heidelberg.

[27] Nguyen-Schäfer, H. Rotordynamics of Automotive Turbochargers. Second Edition. Ludwigsburg, Germany: Springer, 2015. ISBN 978-3-319-17643-7. p.11-14.

[28] Nishimura M, Sugimura T, Yamaguchi A. Three-Dimensional CFD Analysis of the Oil Film in Journal Bearings Considering Cavitation. J Tribol. 1999;121(2):315-22.

[29] Novotný P, Jonák M, Vacula J. Evolutionary optimisation of the thrust bearing considering multiple operating conditions in turbomachinery. International Journal of Mechanical Sciences. 2021 Apr 1; 195:106240. p.2.

[30] Novotný P, Jonák M, Vacula J. Evolutionary optimisation of the thrust bearing considering multiple operating conditions in turbomachinery. International Journal of Mechanical Sciences. 2021 Apr 1; 195:106240. p.4.

[31] Novotný P, Jonák M, Vacula J. Evolutionary optimisation of the thrust bearing considering multiple operating conditions in turbomachinery. International Journal of Mechanical Sciences. 2021 Apr 1; 195:106240. p.5.

[32] Novotný P, Jonák M, Vacula J. Evolutionary optimisation of the thrust bearing considering multiple operating conditions in turbomachinery. International Journal of Mechanical Sciences. 2021 Apr 1; 195:106240. p.7-9.

[33] Novotný P. Hydrodynamic Oil-film Bearings Optimization under Multiple Operating Conditions. 2023 Jan 1; p.1-9.

[34] Peixoto TF, Cavalca KL. A review on the rotor dynamics of automotive turbochargers. In: Parikyan T, editor. Advances in engine and powertrain research and technology. Mechanisms and Machine Science. Cham: Springer; 2022. p. 97-126.

[35] Qiu M, Chen L, Li Y, Yan J. Bearing tribology: principles and applications. Springer; 2016 Oct 20. Chapter 5: “Sliding Bearing Lubrication Theory,” pp. 101-117.

[36] Schommers J, Scheib H, Hartweg M, Bosler A. Minimising friction in combustion engines. MTZ worldwide. 2013 Jul;74(7):28-35.

[37] Shenoy SB, Pai RS, Rao DS, Pai RB. Elasto-hydrodynamic lubrication analysis of full 360'journal bearing using CFD and FSI techniques. World Journal of Modelling and Simulation. 2009;5(4):315-20.

[38] Stachowiak G, Batchelor AW. Engineering Tribology. 4th ed. Butterworth-Heinemann; 2014. Hydrodynamic lubrication. Pages 105-119.

[39] Stachowiak G, Batchelor AW. Engineering Tribology. 4th ed. Butterworth-Heinemann; 2014. p. 11-49.

[40] Stachowiak G, Batchelor AW. Engineering Tribology. 4th ed. Butterworth-Heinemann; 2014. p. 152-169.

[41] Stachowiak G, Batchelor AW. Meaning of Tribology. In: Engineering Tribology. 4th ed. Butterworth-Heinemann; 2014 Sep 16. p. 2-3.

[42] Tanaka M, Hori Y. Thermo-Hydrodynamic Analysis of Journal Bearings by the Finite Element Method Including Mass Conserving Cavitation Algorithm. Tribol Int. 2006;39(12):1450-6.

[43] Tashima S, Taqdokoro T, Tadokoro T, Okimoto H, Niwa Y. Development of sequential twin turbo system for rotary engine. SAE transactions. 1991 Jan 1:900-9.

[44] Usman A, Park CW. Numerical optimization of surface texture for improved tribological performance of journal bearing at varying operating conditions. Industrial Lubrication and Tribology. 2018 Nov 19;70(9):1608-18.

[45] Walkingshaw J, Iosifidis G, Scheuermann T, Filsinger D, Ikeya N. A Comparison of a Mono, Twin and Double Scroll Turbine for Automotive Applications. In: Proceedings of the ASME Turbo Expo 2015: Turbine Technical Conference and Exposition. Volume 8: Microturbines, Turbochargers and Small Turbomachines; Steam Turbines. Montreal, Quebec, Canada; June 15–19, 2015. Paper V008T23A017. ASME.

[46] Walsham BE, Winterbone DE. The Turbocharger. In: Internal Combustion Engineering: Science & Technology. Dordrecht: Springer Netherlands; 1990. p. 615-706.

[47] Wang L, Guo S, Wei Y, Yuan G, Geng H. Optimization research on the lubrication characteristics for friction pairs surface of journal bearings with micro texture. Meccanica. 2019 Jun 1; 54:1135-48.

[48] Wang S, Zhou H, Liu Y. Material properties and their effects on EHD lubrication in journal bearings. Tribol Trans. 2021;64(4):700-710.

[49] Wang X, Li H, Lu W, Meng G. Stiffness and damping properties of (semi) floating ring bearing using magnetorheological fluids as lubricant. Journal of Tribology. 2017 Sep 1;139(5):051701.

[50] Watson N, Janota MS. Introduction to Turbocharging and Turbochargers. In: Turbocharging the Internal Combustion Engine. Palgrave, London; 1982. p.1-2.

[51] Xu X, Zhao H, Li B. Enhanced numerical methods for elastohydrodynamic lubrication in journal bearings. Tribol Lett. 2022; 70:103.

[52] Zhang Q, Wang L. A finite element approach to EHD lubrication analysis of journal bearings. J Tribol. 2021;143(2):021703.

[53] Zhu W, Tang J, Li Z. Numerical analysis of elastohydrodynamic lubrication in journal bearings. Tribol Int. 2021; 154:106721.

Nomenclature

Symbol	Units	Description
p	Pa	Pressure
τ	Pa	Shear stress
u	m/s	Velocity of fluid on x axis
v	m/s	Velocity of fluid on y axis
h	m	Oil film thickness
η	$\mathrm{Ns/m^2}$	Dynamic viscosity
C	[-]	Integration constant

U	$\mathrm{m/s}$	Velocity of fluid on x axis under specific boundary condition
V	$\mathrm{m/s}$	Velocity of fluid on y axis under specific boundary condition
q	$\frac{\mathrm{m^3}}{\mathrm{s}}$	Oil flow in the column
w	$\frac{\mathrm{m}}{\mathrm{s}}$	up-moving speed of an oil in the column
b	m	Width of the bearing
d	m	Diameter
D	m	Bush diameter
c	m	Radial clearance of the bearing
r	m	Radius of the journal
R	m	Radius of the bush
O	[-]	Centre
φ	rad	Shaft rotation angle
h_0	m	Minimal film thickness
e	m	Eccentricity
ε	[-]	Relative eccentricity
ω	$\frac{\mathrm{rad}}{\mathrm{s}}$	Angular velocity

γ'	$\frac{\text{rad}}{\text{s}}$	The angular speed of minimum gap position changing
γ	rad	Minimum gap angle
ε'	s^{-1}	rate of change of the relative eccentricity
F	N	Force
β	rad	Attitude angle
μ	[-]	Friction coefficient
Q	$\frac{\text{m}^3}{\text{s}}$	Volume flow rate
$\dot{\text{m}}$	$\frac{\text{Kg}}{\text{s}}$	Oil mass flow
ρ	$\frac{\text{Kg}}{\text{m}^3}$	Oil density
E	W	Power
M	Nm	Torque
c_p	$\frac{\text{J}}{\text{Kg℃}}$	Specific heat capacity
T	℃	Temperature
W	[-]	Weight factor
n	rpm	Rotor speed
N	[-]	number of operating conditions
S_p	[-]	Pressure factor

S_h	[-]	film thickness factor
λ	[-]	Power exponent

Indexes

x	Direction on x axis
y	Direction on y axis
z	Direction on z axis
0	Bottom of the fluid column
h	Top of the fluid column
b	Bush
s	Shaft
e	Effective
p	Pivot
max	Maximum
in	Inlet
r	Radial
t	Tangential
f	Friction
pr	Pressurised
c	Couette
br	Bore
out	Outlet
$init$	Initial

obj	Objective
ftr	Friction torque ratio
lim	Limit

Abbreviatures

RPM	Rotation per minute
VGS	Turbo with variable geometry
VGT	Variable geometry turbocharger
VNT	Variable nozzle turbo
VTG	Variable turbine geometry
VGS	Variable geometry system
VTA	Variable turbine area
RFRB	rotating floating ring bearing
SFRB	semi-floating ring bearing
CFD	computational fluid dynamics
EHD	elasto-hydrodynamics
$const$	Constant value
1D	One dimensional
2D	Two dimensional
3D	Three dimensional
HPC	High-performance computing
FEM	Finite elements method
GA	Genetic algorithms
VUT	Brno university of technology